Article

Molecular Cell

PTEN Suppresses Glycolysis by Dephosphorylating and Inhibiting Autophosphorylated PGK1

Graphical Abstract

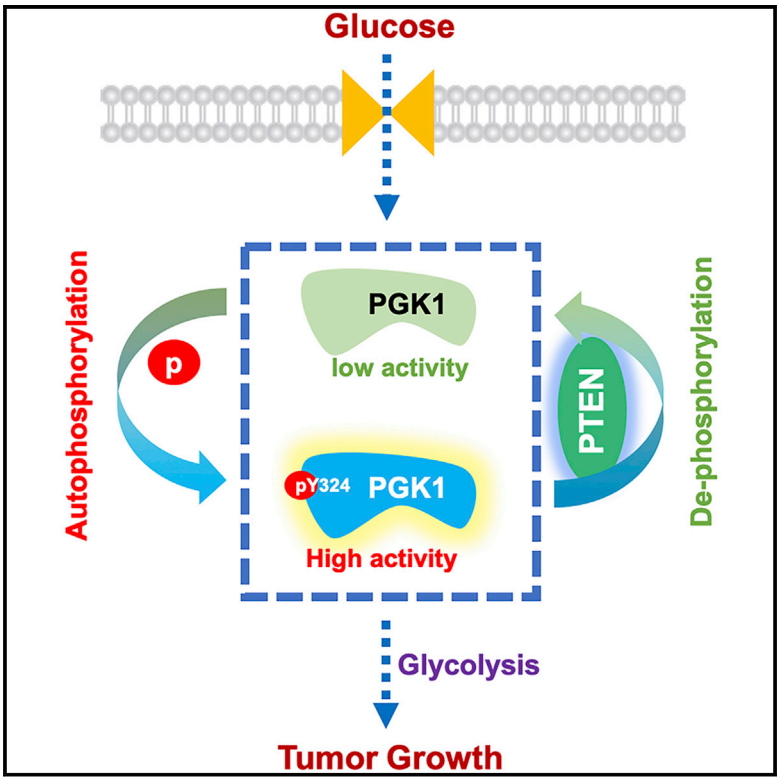

Authors

Xu Qian, Xinjian Li, Zhumei Shi, ..., Tao Jiang, Haitao Li, Zhimin Lu

Correspondence

xqianmedres@njmu.edu.cn (X.Q.), zhiminlu@zju.edu.cn (Z.L.)

In Brief

Qian et al. demonstrate that PGK1 functions as a protein kinase and autophosphorylates itself at Y324, leading to subsequent PGK1 activation. This phosphorylation is dephosphorylated by the protein phosphatase activity of PTEN. Loss of PTEN expression in tumors enhances PGK1 activity, thereby promoting glycolysis and brain tumor growth.

Highlights

- PGK1, functioning as a protein kinase, autophosphorylates itself at Y324
- PGK1 autophosphorylation enhances its glycolytic activity via promoting ATP release
- PTEN, functioning as a protein phosphatase, dephosphorylates PGK1 pY324
- PGK1 Y324 autophosphorylation promotes brain tumor formation

Qian et al., 2019, Molecular Cell *76*, 1–12
November 7, 2019
https://doi.org/10.1016/j.molcel.2019.08.006

CellPress

Please cite this article in press as: Qian et al., PTEN Suppresses Glycolysis by Dephosphorylating and Inhibiting Autophosphorylated PGK1, Molecular Cell (2019), https://doi.org/10.1016/j.molcel.2019.08.006

Molecular Cell
Article

PTEN Suppresses Glycolysis by Dephosphorylating and Inhibiting Autophosphorylated PGK1

Xu Qian,[1,2,3,14,*] Xinjian Li,[4,14] Zhumei Shi,[5] Yan Xia,[3] Qingsong Cai,[3] Daqian Xu,[3] Lin Tan,[6] Linyong Du,[7] Yanhua Zheng,[3] Dan Zhao,[8,9] Chuanbao Zhang,[10] Philip L. Lorenzi,[6] Yongping You,[2,5] Bing-Hua Jiang,[11,12] Tao Jiang,[10] Haitao Li,[8,9] and Zhimin Lu[13,15,*]

[1]Department of Epidemiology, Center for Global Health, School of Public Health, Nanjing Medical University, Nanjing, Jiangsu 211166, China
[2]Institute for Brain Tumors, Jiangsu Key Lab of Cancer Biomarkers, Prevention, and Treatment, Jiangsu Collaborative Innovation Center for Cancer Personalized Medicine, Nanjing Medical University, Nanjing, Jiangsu 211166, China
[3]Brain Tumor Center and Department of Neuro-Oncology, The University of Texas MD Anderson Cancer Center, Houston, TX 77030, USA
[4]CAS Key Laboratory of Infection and Immunity, CAS Center for Excellence in Biomacromolecules, Institute of Biophysics, Chinese Academy of Sciences, Beijing 100101, China
[5]Department of Neurosurgery, The First Affiliated Hospital of Nanjing Medical University, Nanjing, Jiangsu 210029, China
[6]Department of Bioinformatics & Computational Biology, Proteomics and Metabolomics Core Facility, The University of Texas MD Anderson Cancer Center, Houston, TX 77030, USA
[7]School of Laboratory Medicine and Life Science, Wenzhou Medical University, Wenzhou, Zhejiang 325035, China
[8]MOE Key Laboratory of Protein Sciences, Beijing Advanced Innovation Center for Structural Biology, Department of Basic Medical Sciences, School of Medicine, Tsinghua University, Beijing 100084, China
[9]Tsinghua-Peking Center for Life Sciences, Tsinghua University, Beijing 100084, China
[10]Beijing Neurosurgical Institute, Capital Medical University, Beijing 100050, China
[11]The First Affiliated Hospital of Zhengzhou University, Zhengzhou University, Zhengzhou, Henan 450052, China
[12]Department of Pathology, University of Iowa, Iowa City, IA 52242, USA
[13]Zhejiang Provincial Key Laboratory of Pancreatic Disease, The First Affiliated Hospital, and Institute of Translational Medicine, Zhejiang University School of Medicine, Hangzhou, Zhejiang 310029, China
[14]These authors contributed equally
[15]Lead Contact
*Correspondence: xqianmedres@njmu.edu.cn (X.Q.), zhiminlu@zju.edu.cn (Z.L.)
https://doi.org/10.1016/j.molcel.2019.08.006

SUMMARY

The PTEN tumor suppressor is frequently mutated or deleted in cancer and regulates glucose metabolism through the PI3K-AKT pathway. However, whether PTEN directly regulates glycolysis in tumor cells is unclear. We demonstrate here that PTEN directly interacts with phosphoglycerate kinase 1 (PGK1). PGK1 functions not only as a glycolytic enzyme but also as a protein kinase intermolecularly autophosphorylating itself at Y324 for activation. The protein phosphatase activity of PTEN dephosphorylates and inhibits autophosphorylated PGK1, thereby inhibiting glycolysis, ATP production, and brain tumor cell proliferation. In addition, knockin expression of a PGK1 Y324F mutant inhibits brain tumor formation. Analyses of human glioblastoma specimens reveals that PGK1 Y324 phosphorylation levels inversely correlate with PTEN expression status and are positively associated with poor prognosis in glioblastoma patients. This work highlights the instrumental role of PGK1 autophosphorylation in its activation and PTEN protein phosphatase activity in governing glycolysis and tumorigenesis.

INTRODUCTION

The phosphatase and tensin homolog (PTEN) tumor suppressor is one of the most frequently altered genes in cancer (Li et al., 1997; Steck et al., 1997). PTEN regulates a wide array of cellular processes, including survival, proliferation, energy metabolism, and cellular architecture (Song et al., 2012). PTEN dephosphorylates phosphatidylinositol-3,4,5-trisphosphate (PI[3,4,5]P3), an activator of 3-phosphoinositide-dependent kinase (PDK) and AKT. Loss of PTEN function increases levels of PI(3,4,5)P3 and leads to the activation of the phosphoinositide 3-kinase (PI3K)-AKT pathway (Maehama and Dixon, 1998; Stambolic et al., 1998; Sun et al., 1999). Activation of this pathway regulates instrumental cellular activities; it enhances glycolysis through increasing glucose transporter expression and glucose capture by hexokinase and stimulating phosphofructokinase activity (Vander Heiden et al., 2009). It is well known that the Warburg effect, a high rate of glycolysis and lactic acid fermentation even in the presence of ample oxygen, is a feature of most cancer cells (Yang and Lu, 2013, 2015). However, whether PTEN directly regulates the glycolytic pathway is unknown. Besides its intensively studied lipid phosphatase activity, PTEN possesses protein phosphatase activity and dephosphorylates phosphorylated serine, threonine, and tyrosine residues in peptide substrates *in vitro* and in protein substrates, such as focal adhesion kinase, cyclic

AMP (cAMP)-responsive-element-binding protein, insulin receptor substrate, and c-Src, consequently regulating these proteins' functions (Gu et al., 2011; Myers et al., 1997; Shi et al., 2014; Tamura et al., 1998; Zhang et al., 2011).

Phosphoglycerate kinase 1 (PGK1), the first ATP-generating enzyme in the glycolytic pathway, catalyzes the reversible phosphotransfer reaction from the 1 position of 1,3-biphosphoglycerate to ADP, which leads to the generation of 3-phosphoglycerate (3-PG) and ATP (Bernstein and Hol, 1998). By controlling ATP and 3-PG levels, PGK1 is crucial for coordinating energy production with biosynthesis and redox balance (Wang et al., 2015). Aside from its glycolytic activity, PGK1 was recently identified as a protein kinase that phosphorylates pyruvate dehydrogenase kinase 1 at T338 and Beclin1 at S30 to regulate mitochondrial metabolism and autophagy, respectively (Li et al., 2016; Qian et al., 2017a, 2017b). PGK1 expression is upregulated in many types of human cancer, including breast cancer (Zhang et al., 2005), pancreatic ductal adenocarcinoma (Hwang et al., 2006), and radioresistant astrocytoma (Yan et al., 2012), as well as in multidrug-resistant ovarian cancer cells (Duan et al., 2002) and metastatic gastric cancer, colon cancer, and hepatocellular carcinoma cells (Ahmad et al., 2013; Ai et al., 2011; Zieker et al., 2010). Although PGK1 is known to be overexpressed in human cancers and to play a critical role in regulating instrumental cellular activities, how the regulation of PGK1 activity is involved in tumorigenesis is largely unclear.

In this report, we demonstrated that PGK1 is autophosphorylated at Y324 for its activation. PTEN directly interacted with PGK1 and dephosphorylated autophosphorylated PGK1 for inhibition of glycolysis and ATP production. The inhibition of PGK1 autophosphorylation blunted brain tumorigenesis.

RESULTS

PTEN Dephosphorylates Tyrosine-Phosphorylated PGK1

To determine whether PTEN is directly involved in the regulation of glycolysis, we stably expressed wild-type (WT) PTEN or three PTEN mutants in PTEN-deficient U87 or U251 human glioblastoma cells. PTEN C124S is deficient in both lipid and protein phosphatase activities, while PTEN G129E and PTEN Y138L are deficient in lipid phosphatase activity and protein phosphatase activity, respectively (Davidson et al., 2010; Liaw et al., 1997; Wozniak et al., 2017). As expected, WT PTEN and PTEN Y138L, but not PTEN C124S and PTEN G129E mutants, inhibited AKT T308 phosphorylation (Figure S1A). ^{3}H-glucose labeling experiments and lactate measurements demonstrated that the expression of WT PTEN and PTEN Y138L, but not the PTEN C124S mutant, reduced the glucose-glycolytic rate (Figures 1A and S1B) and inhibited lactate production (Figures 1B and S1C). These results are in line with the known function of PTEN lipid phosphatase activity-regulated AKT in glycolysis (Vander Heiden et al., 2009). Expression of the lipid phosphatase-inactive PTEN G129E mutant also had an inhibitory effect on glycolysis, suggesting that the protein phosphatase activities of PTEN also play instrumental roles in glycolysis regulation. Consistent with these results, PTEN-depleted LN229 glioblastoma multiforme (GBM) cells (Figure S1D) and Pten-deficient mouse embryonic fibroblasts (MEFs) (Figure S1E), compared to their endogenous PTEN-expressing counterparts, exhibited an increased glycolytic rate and lactate production. This increase was suppressed to varying degrees by the reconstituted expression of WT PTEN, PTEN G129E, and PTEN Y138L, but not the PTEN C124S mutant. In addition, treatment of U87 cells with the PI3K inhibitor LY294002 or the AKT inhibitor MK-2206 induced a weaker inhibitory effect on glycolysis than did WT PTEN expression (Figure S1F), whereas expression of a constitutively active Myr-AKT mutant (Figure S1G) only partially rescued WT PTEN-inhibited glycolysis (Figure S1H). These results strongly suggested that both the lipid and protein phosphatase activities of PTEN are involved in the regulation of glycolysis.

To identify the mechanism underlying the protein phosphatase activities of PTEN-regulated glycolysis, we immunoprecipitated inactive FLAG-PTEN C124S, which has high substrate binding affinity and acts as a substrate trap (Myers et al., 1998), from U87 cells, performed mass spectrometric analysis of the PTEN-associated proteins, and identified PGK1 as the only glycolytic enzyme bound to PTEN (Table S1). This result was further supported by co-immunoprecipitation analyses, which showed that PTEN C124S bound to endogenous PGK1 in U87 cells and that endogenous PTEN associated with endogenous PGK1 in both LN229 and LN18 GBM cells (Figure 1C). An *in vitro* pull-down assay showed that purified His-PTEN bound to purified glutathione S-transferase (GST)-PGK1 (Figure S1I). Of note, both inactive PTEN C124S and the PTEN-trapping mutant D92A (Tamura et al., 1998) bound to PGK1 much more strongly than did its WT counterpart (Figure S1J). In addition, the binding of PGK1 to WT PTEN, and to a much lesser extent to PTEN C124S or PTEN D92A, was competitively inhibited in a dosage-dependent manner by sodium orthovanadate (Figure S1J), which acts as a phospho-tyrosine mimetic and covalently modifies the catalytic cysteine residue of phosphatases, thereby functioning as a competitive inhibitor of phosphatases (Tiganis and Bennett, 2007). These results suggest that PGK1 is a potential substrate of PTEN.

Immunoblotting analyses of immunoprecipitated PGK1 showed that the tyrosine phosphorylation levels of PGK1, but not those of serine or threonine (data not shown), were substantially increased in Pten-deficient MEFs (Figure 1D). This increase was suppressed by reconstituted expression of WT PTEN and PTEN G129E, but not PTEN C124S or PTEN Y138L (Figure 1E), suggesting that the protein but not the lipid phosphatase activities of PTEN regulate PGK1 tyrosine phosphorylation. In line with this finding, analyses of a panel of human GBM cell lines showed that PGK1 tyrosine phosphorylation levels were higher in PTEN-deficient U87, U251, A172, and D54 cells than in WT PTEN-expressing LN229 and LN18 cells (Figure 1F; Lee et al., 2011; Wick et al., 1999). These results indicated that PTEN regulates PGK1 tyrosine phosphorylation.

PGK1 Is Autophosphorylated at Y324

PGK1 has been identified as a protein kinase (Li et al., 2016; Qian et al., 2017a), and it is known that some protein kinases can autophosphorylate for the regulation of their activities and functions (Lu and Hunter, 2009). We next performed protein

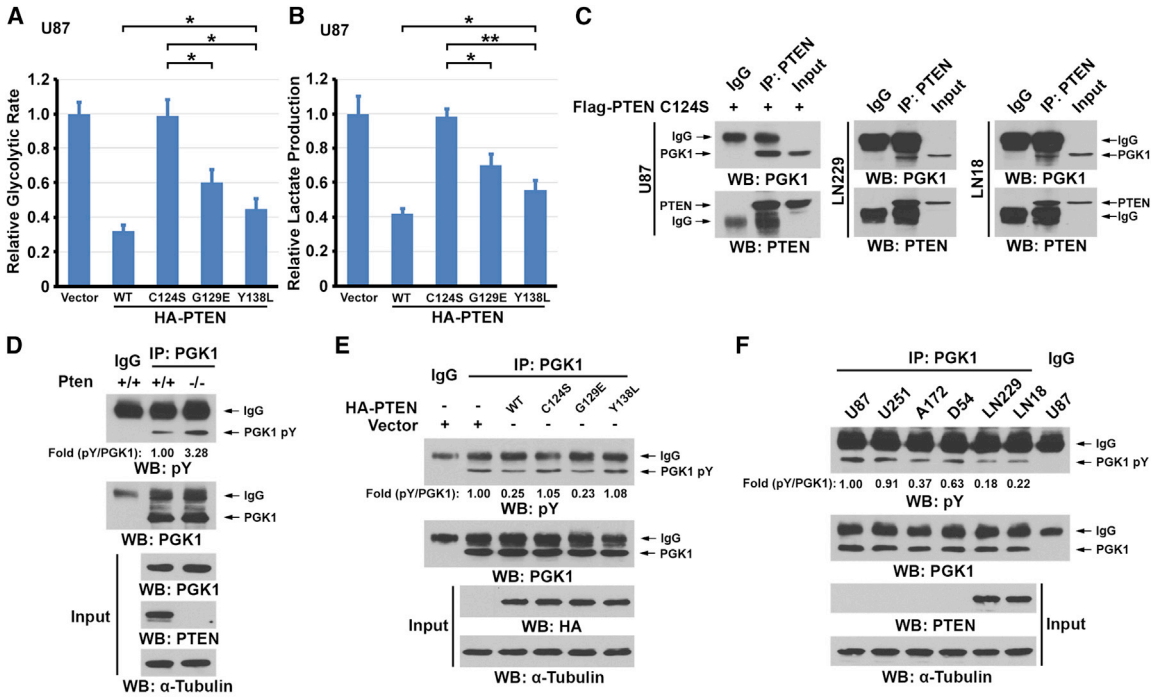

Figure 1. PTEN Dephosphorylates Tyrosine-Phosphorylated PGK1

(A and B) U87 cells with or without stably expressing HA-tagged WT PTEN, PTEN C124S, PTEN G129E, or PTEN Y138L mutant was cultured. Cells were incubated with D-[5-^{3}H]-glucose (10 μCi) for 1 h. The glycolytic rate was determined by measuring $^{3}H_2O$ converted from D-[5-^{3}H]-glucose via scintillation counting (H_2O is generated from 2-phosphoglycerate by enolase, which is downstream of the PGK1-mediated reaction) (A). Lactate production was measured (B). The data represent the means ± SDs of triplicate experiments. *$p < 0.05$ and **$p < 0.001$.

(C) Immunoprecipitation with an anti-PTEN antibody and immunoblotting analyses with the indicated antibodies were performed using U87 cells (left panel) transfected with FLAG-tagged PTEN C124S mutant or endogenous PTEN-expressing LN229 (middle panel) or LN18 (right panel) cells.

(D–F) Immunoprecipitation of endogenous PGK1 with an anti-PGK1 antibody and immunoblotting analyses with the indicated antibodies were performed. Pten$^{+/+}$ or Pten$^{-/-}$ MEFs were cultured and lysed (D). HA-tagged WT PTEN, PTEN C124S, PTEN G129E, or PTEN Y138L mutant was expressed in Pten$^{-/-}$ MEFs (E). The indicated GBM cells were cultured and lysed. Intensities of pY relative to the corresponding PGK1 levels were quantified and normalized to the first group (F). pY, antibody against phosphorylated tyrosine.

phosphorylation assays by incubating [γ-^{32}P]-ATP with purified recombinant His-PGK1 or a catalytically inactive His-PGK1 T378P mutant and showed that only WT His-PGK1 was phosphorylated (Figure S2A). Liquid chromatography-coupled Orbitrap mass spectrometry (LC-MS/MS) analyses of tryptic digests of PGK1 showed that PGK1 was autophosphorylated at evolutionarily conserved tyrosine (Y) 324 (Figures S2B and S2C). Mutation of Y324 into phenylalanine (F) rendered PGK1 resistant to autophosphorylation *in vitro* as detected using autoradiography with [γ-^{32}P]-ATP (Figure 2A, left panel) and a specific anti-phospho-PGK1 Y324 antibody (Figures 2A, right panel, and S2D). In addition, PGK1 Y324 was highly phosphorylated in Pten-deficient MEFs but not in their WT counterparts (Figure 2B, left panel). Furthermore, WT FLAG-PGK1, but not FLAG-PGK1 Y324F, was autophosphorylated in U87 and U251 cells (Figure 2B, right panel). These results indicated that PGK1 is autophosphorylated at Y324. Given that the Michaelis-Menten constant (K_M) of ATP (0.23 ± 0.031 mM) for PGK1 autophosphorylation (Figure S2E) is much lower than the physiological concentrations of ATP (1–5 mM) in cancer cells (Lane and Fan, 2015), these results suggested that PGK1 is efficiently autophosphorylated in cancer cells.

To determine whether PGK1 autophosphorylation occurs inter- or intramolecularly, we performed an His pull-down assay and showed that purified GST-PGK1 interacted with purified His-PGK1 (Figure 2C). This finding was confirmed *in vivo* by co-immunoprecipitation assays showing that FLAG-tagged PGK1 associated with hemagglutinin (HA)-tagged PGK1 in both U87 and U251 cells (Figure S2F). Purified WT His-PGK1 phosphorylated a GST-PGK1 T378P kinase-dead mutant (Figure 2D), and this phosphorylation was increased in a PGK1 T378P dosage-dependent manner (Figure 2E). In contrast, PGK1 autophosphorylation was inhibited in a dosage-dependent manner by purified PGK1 Y324F/T378P (Figure 2E). These results strongly suggested that PGK1 is intermolecularly autophosphorylated and releases its substrate once phosphorylation is complete, whereas the PGK1 Y324F/T378P phosphorylation-dead mutant binds to WT His-PGK1 and blocks WT His-PGK1 transphosphorylation. Consistent with these *in vitro* results, the reduction of endogenous PGK1 expression by expressing PGK1 short hairpin RNA (shRNA) in U87 cells reduced endogenous PGK1-dependent phosphorylation of S protein-FLAG-streptavidin-binding peptide (SFB)-tagged and RNAi-resistant (r) PGK1 T378P. This inhibition was rescued by expression of

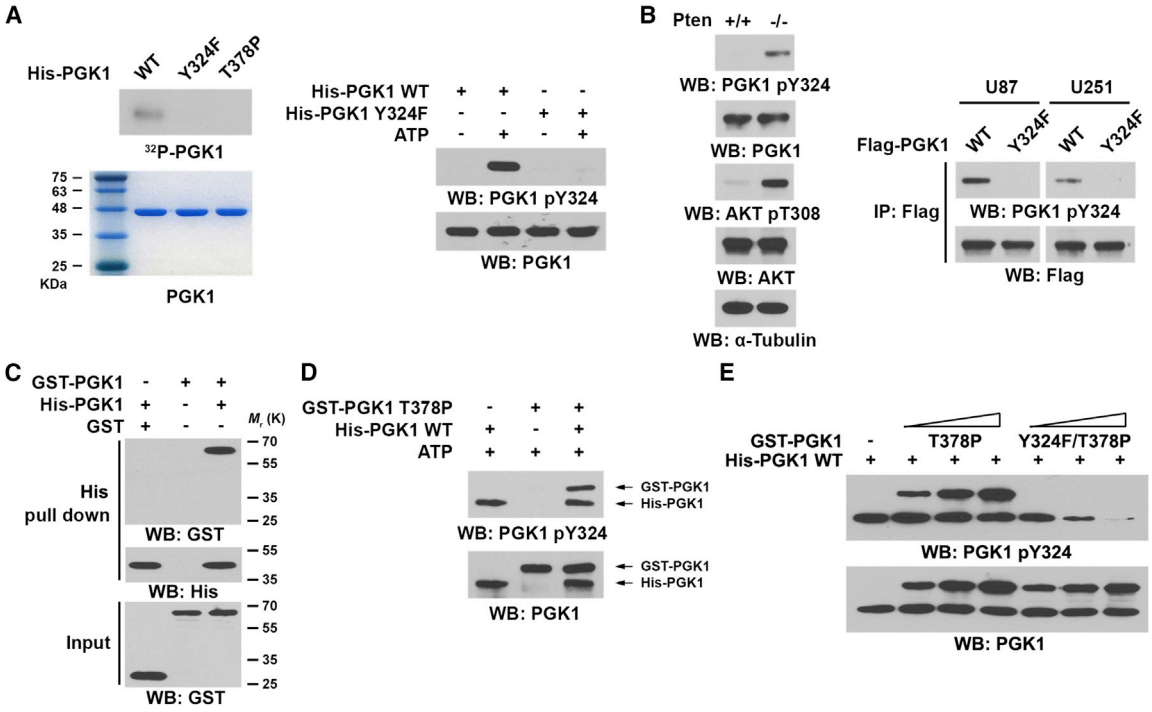

Figure 2. PGK1 Is Autophosphorylated at Y324

Immunoprecipitation and immunoblotting analyses were performed with the indicated antibodies.

(A) Purified WT His-PGK1, His-PGK1 Y324F, or His-PGK1 T378P mutant was incubated in the presence of [γ-^{32}P]-ATP. Autoradiography was performed (left, top panel). Coomassie blue staining of protein is shown (left, bottom panel). Purified His-PGK1 was phosphorylated *in vitro* and immunoblotted with an anti-PGK1 pY324 antibody (right panel).

(B) Pten$^{+/+}$ or Pten$^{-/-}$ MEFs were lysed (left panel). FLAG-tagged WT PGK1 or PGK1 Y324F mutants were expressed in U87 or U251 cells (right panel).

(C) An His pull-down assay with nickel-nitrilotriacetic acid (Ni-NTA) agarose beads was performed by mixing bacterially purified GST or GST-PGK1 with bacterially purified His-PGK1. His-PGK1 did not bind to GST control protein.

(D) An *in vitro* kinase assay was performed by mixing bacterially purified WT His-PGK1 and bacterially purified GST-PGK1 T378P mutant.

(E) An *in vitro* kinase assay was performed by mixing the bacterially purified WT His-PGK1 with or without bacterially purified GST-PGK1 T378P or GST-PGK1 Y324F/T378P mutant for 1 min.

WT HA-rPGK1 but not HA-rPGK1 T378P (Figure S2G). These results strongly suggested that PGK1 is autophosphorylated intermolecularly.

Autophosphorylated PGK1 Is Dephosphorylated by PTEN

PTEN regulates PGK1 tyrosine phosphorylation (Figures 1D and 1E). We next determined whether PTEN directly dephosphorylates PGK1 pY324. Similar to the relation between PTEN status and PGK1 tyrosine phosphorylation levels in GBM cells (Figure 1F), PGK1 pY324 levels were higher in PTEN-deficient U87, U251, A172, and D54 cells than in WT PTEN-expressing LN229 and LN18 cells (Figure 3A). As expected, PI(3,4,5)P3 was dephosphorylated by purified WT PTEN and by lipid phosphatase activity-intact PTEN Y138L, but not by PTEN C124S or PTEN G129E mutants (Figure S3A). In contrast, a PGK1-pY324 peptide, an acidic standard PTEN substrate poly-(EY) peptide (Myers et al., 1997; Figure S3B), and purified His-PGK1 protein (Figure 3B) were dephosphorylated by WT PTEN and the protein phosphatase activity-intact PTEN G129E mutant, but not by PTEN C124S or PTEN Y138L mutants. Comparable kinetic parameters (K_M and catalytic rate constant [k_{cat}]) of the dephosphorylation of PGK1-pY324 and poly-(EY) peptides were observed (Figure S3C). In addition, the expression of WT PTEN and the PTEN G129E mutant, but not PTEN C124S or PTEN Y138L, dephosphorylated PGK1 at pY324 in both U87 (Figure 3C) and U251 cells (Figure S3D). Furthermore, doxycycline-induced expression of PTEN shRNA in LN229 cells enhanced PGK1 Y324 phosphorylation (Figure 3D). Consistently, CRISPR-Cas9-mediated knockout of PTEN and knockin expression of PTEN Y138L in LN229 cells greatly increased PGK1 Y324 phosphorylation (Figure S3E). In contrast, overexpression of other protein tyrosine phosphatases, such as PTP-PEST, receptor protein tyrosine phosphatase α (RPTPα), Src homology region 2 domain-containing phosphatase 1 (SHP1), and SHP2, failed to regulate PGK1 Y324 phosphorylation (Figures S3F–S3H). In addition, neither hypoxia (1% O_2) treatment nor serum stimulation altered PTEN-mediated PGK1 Y324 dephosphorylation (Figures S3I and S3J). Furthermore, hypoxia-induced PGK1 S203 phosphorylation, which mediates mitochondrial translocation of PGK1 (Li et al., 2016), did not alter PGK1 Y324 phosphorylation, and vice versa (Figure S3K). These data suggested that PTEN is a protein phosphatase for Y324-autophosphorylated PGK1.

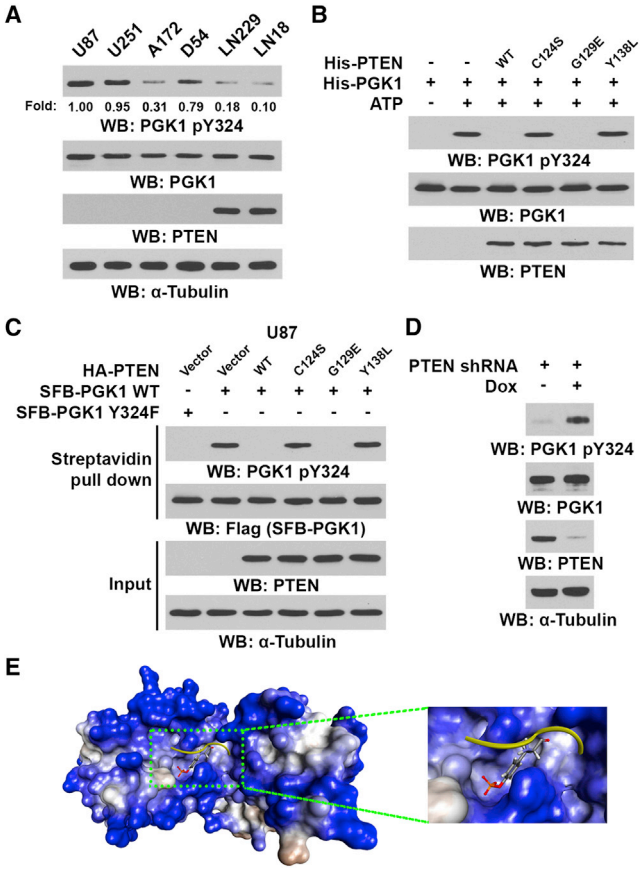

Figure 3. Autophosphorylated PGK1 Is Dephosphorylated by PTEN

(A–D) Immunoblotting analyses were performed with the indicated antibodies.

(A) The indicated GBM cells were cultured and lysed.

(B) Purified His-PGK1 immobilized on Ni-NTA agarose beads was incubated with or without ATP, followed by washing with PBS and incubation with or without purified WT His-PTEN, His-PTEN C124S, His-PTEN G129E, or PTEN Y138L mutant.

(C) SFB-tagged WT PGK1 or PGK1 Y324F mutant with or without HA-tagged WT PTEN, PTEN C124S, PTEN G129E, or PTEN Y138L mutant were expressed in U87 cells. A streptavidin pull-down assay was performed.

(D) LN229 cells stably expressing doxycycline (Dox)-inducible PTEN shRNA were incubated with or without Dox (1 μg/mL) for 3 days.

(E) Docking analysis of PTEN (PDB: 1D5R) with Y324-phosphorylated PGK1 peptide (321-SKKpYAEA-327), which is shown as backbone in yellow, while pY324 is shown with colored balls and sticks.

We next performed molecular docking analyses of PTEN with the Y324-phosphorylated PGK1 peptide (321-SKKpYAEA-327) and showed that phosphorylated PGK1 peptide can be accommodated into the catalytic pocket of PTEN (Figure 3E). Furthermore, we revealed a 3.5-Å distance between the $-PO_3$ group of the phosphorylated PGK1 peptide and the $-SH$ group of cysteine (C) 124 of PTEN (Figure S3L), indicating that PTEN could feasibly dephosphorylate PGK1. These results indicated that PTEN dephosphorylates autophosphorylated PGK1 at Y324.

PTEN Inhibits Autophosphorylation-Activated PGK1

To determine the effect of PGK1 autophosphorylation and the regulation by PTEN of this autophosphorylation on PGK1 activity, we measured PGK1 activity *in vitro* and showed that purified PGK1 Y324F and inactive PGK1 T378P mutants exhibited greatly reduced activity compared to their WT counterpart, which was autophosphorylated in the presence of ATP and Mg^{2+} (Figure 4A). In addition, purified autophosphorylated PGK1, compared to purified nonphosphorylated WT PGK1, PGK1 Y324F, or PGK1 T378P, had greatly increased binding of a ^{14}C-labeled ADP substrate (Figure 4B). Furthermore, the PGK1 Y324F mutant yielded a much lower V_{max} and much higher K_M toward its substrates (ATP and 3-PG) than did its WT counterpart (Figure S4A). In line with these findings, PGK1 activities were positively correlated with PGK1 Y324 phosphorylation levels in GBM cells (Figures 3A and S4B). Knockout of PTEN and knockin expression of PTEN Y138L in LN229 cells largely increased PGK1 activity (Figure S4C). These results indicated that PGK1 autophosphorylation increases PGK1 activity.

PGK1 exists in fully open or transiently closed conformations for catalysis, during which the rapid diffusion of substrates and products into and out of the binding sites occurs (Zerrad et al., 2011). To better understand how autophosphorylation promotes the glycolytic activity of PGK1, we used molecular dynamic simulations to compare the structural dynamics of nonphosphorylated and Y324-phosphorylated PGK1 in a fully closed conformation (PDB: 2Y3I) and examined the binding status of the ATP product. The analysis of structural changes in the PGK1 backbone showed that Y324 phosphorylation conferred a more dynamic conformation (with changes evident starting at ~8.0 ns), whereas nonphosphorylated PGK1 remained stable (Figure S4D). A comparison of the fluctuation of PGK1 amino acid residues showed greater conformational variations in Y324-phosphorylated PGK1 than in nonphosphorylated PGK1 (Figure S4E), suggesting that residues in Y324-phosphorylated PGK1 are generally more flexible than those in nonphosphorylated PGK1. The most significantly changed amino acids in Y324-phosphorylated PGK1 were leucine (L) 201, aspartic acid (D) 293, glutamic acid (E) 294, and E346 (Figure S4E). L201 is located in the hinge-bending area, which links the N- and C-terminal arms of PGK1, while D293, E294, and E346 are located in the ATP binding area (Figure S4F). Consistently, the hinge-bending area and the ATP binding area were the most dramatically altered in Y324-phosphorylated PGK1 compared to nonphosphorylated PGK1 (Figure S4G). We analyzed structural differences at 8.5 ns, when conformational differences were present between Y324-phosphorylated and nonphosphorylated PGK1 (Figure S4D). The distance between the N- and C-terminal arms of PGK1, represented by lysine (K) 30 in the N-terminal arm and E344 in the C-terminal arm, was ~8.7 Å in Y324-phosphorylated PGK1 and ~3.7 Å in nonphosphorylated PGK1 (Figure S4H), suggesting a much more "open" status in Y324-phosphorylated PGK1 than in its nonphosphorylated counterpart. Consequently, these conformational changes created an "open channel" in the ATP-binding area that favored ATP release in Y324-phosphorylated PGK1, whereas ATP was "locked" in nonphosphorylated PGK1 (Figure 4C). Calculation of the free energy of binding (ΔG) using the molecular mechanics-generalized Born surface area (MM-GBSA) method revealed that ΔG of ATP binding was much greater for

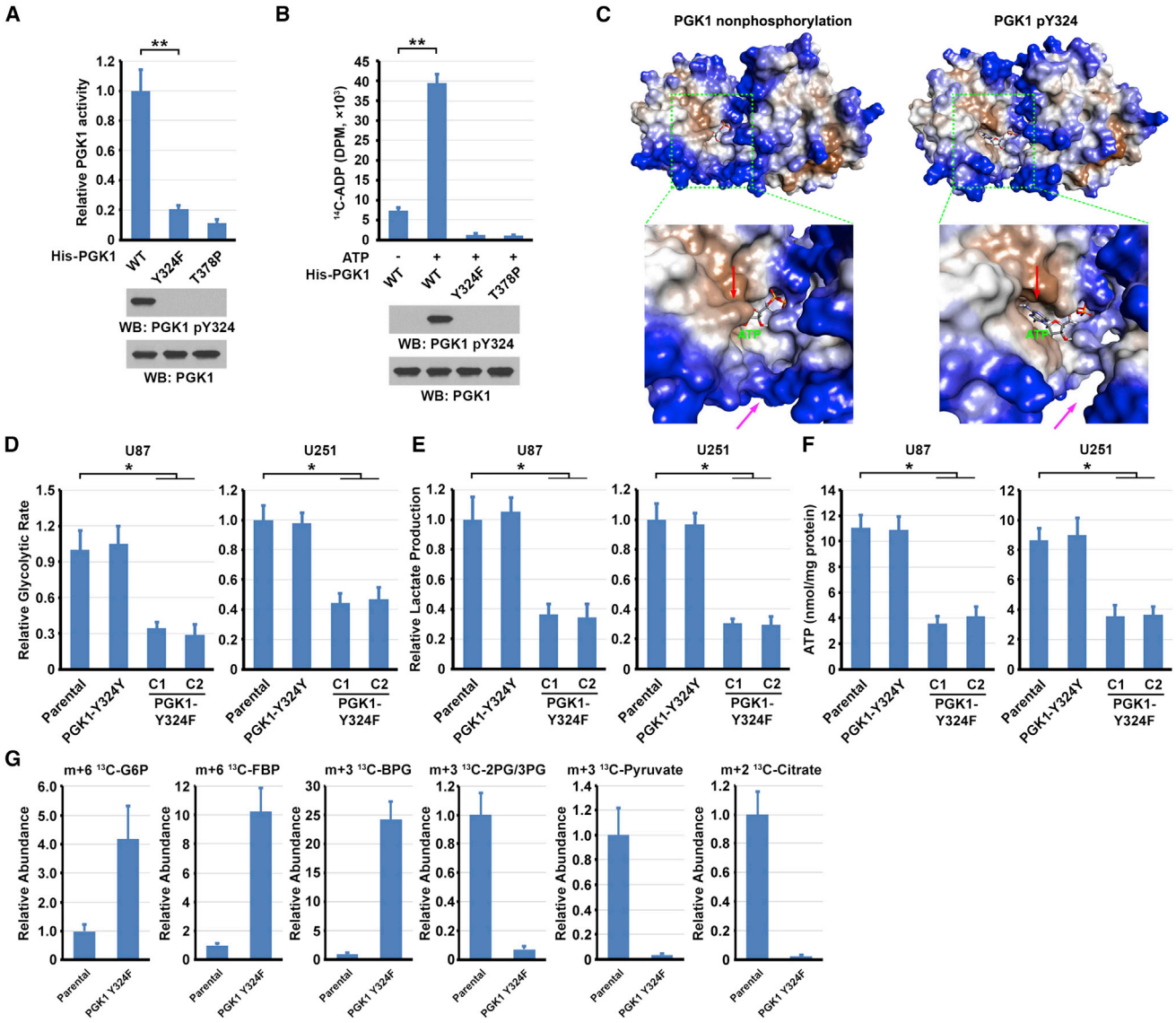

Figure 4. PTEN Inhibits Autophosphorylation-Activated PGK1

(A) WT His-PGK1, His-PGK1 Y324F, or His-PGK1 T378P mutant proteins were incubated in the presence of ATP for 5 min, followed by immunoblotting analyses with the indicated antibodies (bottom panel). PGK1 activity was measured using ATP as substrates (top panel). The data represent the means ± SDs of triplicate experiments. **$p < 0.001$.

(B) WT His-PGK1, His-PGK1 Y324F, or His-PGK1 T378P mutant proteins were incubated with or without ATP for 30 min. The phosphorylated or non-phosphorylated PGK1 protein was either analyzed by immunoblotting analyses with the indicated antibodies (bottom panel) or incubated with ^{14}C-ADP. PGK1-bound ^{14}C-ADP was measured (top panel). The data represent the means ± SDs of triplicate experiments. **$p < 0.001$.

(C) Structural view of nonphosphorylated and Y324-phosphorylated PGK1 generated from molecular dynamic simulation. Red and magenta arrows indicate the closed and open conformations in the ATP-binding area of nonphosphorylated (left panel) and Y324-phosphorylated PGK1 (right panel), respectively.

(D) U87 (left panel) and U251 (right panel) cells with or without PGK1 Y324Y or PGK1 Y324F knockin were incubated with D-[5-^{3}H]-glucose (10 μCi) for 1 h. The glycolytic rate was determined. Data represent the means ± SDs of triplicate experiments. *$p < 0.05$. C1, clone 1; C2, clone 2.

(E and F) Lactate production (E) or ATP concentration (F) was determined in U87 (left panel) and U251 (right panel) cells with or without PGK1 Y324Y or PGK1 Y324F knockin expression. The data represent the means ± SDs of triplicate experiments. *$p < 0.05$.

(G) U87 cells with or without PGK1 Y324F knockin expression were cultured in the presence of 10 mM $^{13}C_6$-glucose for 30 min. ^{13}C-labeled metabolites in glycolysis and the Krebs cycle were measured by LC/MS-MS. The data represent the means ± SDs of triplicate experiments.

Y324-phosphorylated PGK1 (−111.50 ± 7.07 kcal/mol) than for nonphosphorylated PGK1 (−149.71 ± 10.57 kcal/mol). These results suggested that the ATP binding affinity to Y324-phosphorylated PGK1 is decreased and that ATP releases more readily from Y324-phosphorylated PGK1 than from nonphosphorylated PGK1. Given that the reaction of PGK1 in glycolysis is rate limited by the release of its products, such as ATP (Lallemand et al., 2011), these results suggested that PGK1 autophosphorylation

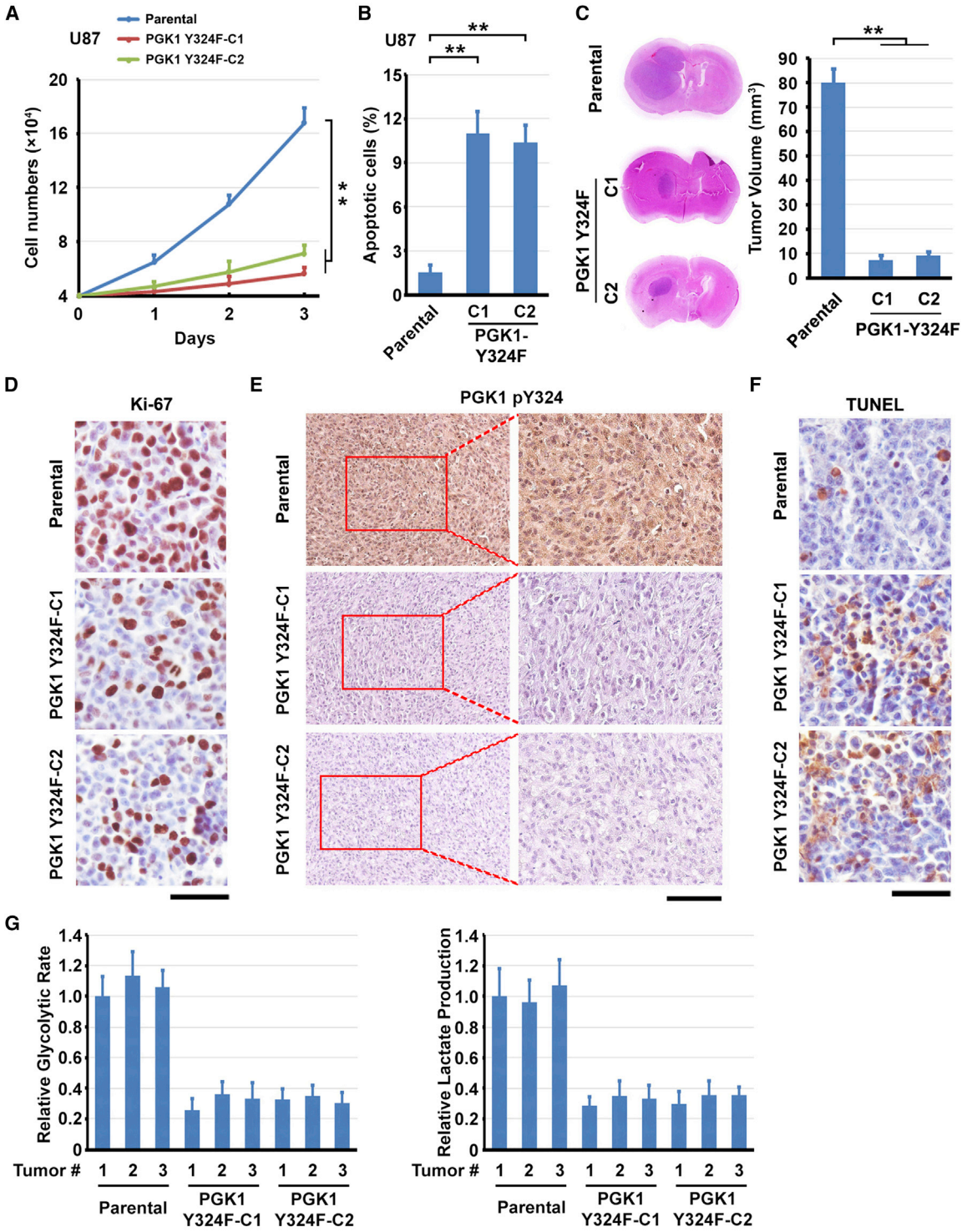

Figure 5. PGK1 Autophosphorylation Is Instrumental for Brain Tumor Growth

(A) U87 cells (4×10^4) with or without PGK1 Y324F knockin were incubated for the indicated period of time. Cell numbers were counted. The data represent the means ± SDs of triplicate samples. **$p < 0.001$.

(B) Apoptosis analyses were performed using U87 cells with or without PGK1 Y324F knockin expression. The data represent the means ± SDs of triplicate experiments. **$p < 0.001$.

(legend continued on next page)

at Y324 induces conformational changes that promote ATP release, thereby increasing PGK1 activity.

To determine the functional consequences of PGK1 Y324 dephosphorylation, we used CRISPR-Cas9 genome editing knockin technology to replace endogenous PGK1 with PGK1 Y324F in U87 cells, U251 cells, Pten$^{+/+}$ MEFs, and Pten$^{-/-}$ MEFs. We also made a silent knockin mutation of PGK1 Y324 (designated PGK1 Y324Y) in U87 (Figure S4I) and U251 (Figure S4J) cells as a control to validate the specific effect induced by PGK1 Y324F expression. We determined the glycolytic rate and the lactate level of these cells. Knockin expression of PGK1 Y324F, but not PGK1 Y324Y, reduced the glycolytic rate (Figures 4D and S4K) and largely inhibited the production of lactate (Figures 4E and S4L) and ATP (Figure 4F) in PTEN-deficient cells. ^{13}C-glucose labeled U87 cells with knockin expression of PGK1 Y324F exhibited an accumulation of PGK1 upstream glycolytic intermediates and a reduction in PGK1 downstream intermediates, such as 2-phosphoglycerate/3-phosphoglycerate (2PG/3PG), pyruvate, and citrate (Figure 4G). In addition, suppression of mitochondrial oxidative phosphorylation was observed in these cells (Figure S4M). Notably, the reduced glycolytic rate was rescued by ectopically expressed WT PGK1 (Figures S4N and S4O) and abundantly overexpressed PGK1 Y324F (Figures S4P and S4Q). The addition of phosphoenolpyruvate (PEP), a downstream metabolite of PGK1, rescued the inhibitory effect of PGK1 Y324F expression on lactate (Figure S4R) and ATP (Figure S4S) production in a dosage-dependent manner, but it did not affect the glycolytic rate, which was determined by measuring ^{3}H-glucose-derived $^{3}H_2O$, a metabolite upstream of PEP (Figure S4R). These results indicated that PTEN-regulated PGK1 activity plays an instrumental role in glycolysis regulation and ATP production.

Glutamine-derived oxaloacetate and malate can be converted to PEP and pyruvate by phosphoenolpyruvate carboxykinase (PEPCK) and malic enzyme, respectively, thereby joining glycolysis (Figure S5A). To examine whether the incorporation of glutamine into glycolysis is affected by PGK1 Y324F expression, we used ^{13}C-glutamine to label U87 cells with or without knockin expression of PGK1 Y324F. We found that the amounts of ^{13}C-PEP, ^{13}C-2-PG/3-PG, ^{13}C-pyruvate, and ^{13}C-lactate in U87 cells with knockin expression of PGK1 Y324F were greater than those in U87 cells with WT PGK1 expression (Figure S5B; Table S2). These results suggest that glutaminolysis partially compensates for the reduced glycolysis induced by PGK1 Y324F expression.

We next determined whether PGK1 Y324 autophosphorylation affects its protein kinase activity. The purified FLAG-PGK1 Y324F mutant phosphorylated the His-PGK1 T378P kinase-dead mutant at Y324 (Figure S5C). In addition, PGK1 Y324F and WT PGK1 exhibited comparable phosphorylation of Beclin1 S30 *in vitro* (Figure S5D). Beclin1 S30 phosphorylation is induced in autophagy initiation (Qian et al., 2017a). Glucose deprivation resulted in S30 phosphorylation of WT Beclin1, but not Beclin1 S30A, at similar levels in U87 cells expressing WT PGK1 and those expressing the PGK1 Y324F mutant (Figure S5E). These results suggested that Y324 autophosphorylation does not regulate the protein kinase activity of PGK1. A computer-based protein-peptide docking analysis demonstrated that a Beclin1 peptide spanning S30 can be accommodated into the open conformation of PGK1 but not the closed conformation (Qian et al., 2017a), suggesting that PGK1 in its open status functions as a protein kinase. In line with this finding, molecular dynamic simulation analyses showed that Y324-phosphorylated PGK1 (PDB: 1VJD, a fully open conformation) in the presence of ATP had no obvious alterations in the ATP binding area (amino acids 285–350) compared to nonphosphorylated PGK1 (Figure S5F). This result suggested that Y324 phosphorylation does not affect the access of ATP to PGK1 in its open conformation or its subsequent protein kinase activity.

We recently showed that the glycolytic activity of PGK1 is important for promoting DNA replication by catalyzing ADP to ATP and alleviating the inhibitory effect of ADP on CDC7-ASK-mediated MCM2 S53 phosphorylation (Li et al., 2018). We found that PGK1 Y324F mutant, which retained its binding ability to CDC7, reduced the phosphorylation level of MCM2 S53 (Figure S5G). These results suggested that PGK1 Y324 phosphorylation affects not only glycolysis but also other important cellular activities.

PGK1 Autophosphorylation Is Instrumental for Brain Tumor Growth

Aerobic glycolysis is critical for tumor cell proliferation. As expected, the knockout of PTEN in LN229 cells greatly enhanced cell proliferation (Figure S6A). Although to a lesser extent, the knockin expression of PTEN Y138L also promoted cell proliferation of LN229 cells (Figure S6A). Compared to limited proliferation inhibition on endogenous PTEN-expressing LN229 cells (Figure S6B) and Pten$^{+/+}$ MEFs (Figure S6C), the knockin expression of PGK1 Y324F greatly inhibited cell proliferation (Figures 5A, S6C, and S6D) and enhanced apoptosis (Figures 5B, S6E, and S6F) in Pten$^{-/-}$ MEFs and PTEN null U87 and U251 cells. This proliferation inhibition was alleviated by supplementing PEP in a dosage-dependent manner (Figure S6G). Consistent results showed that expressing PTEN G129E mutant in U87 cells largely decreased cell proliferation (Figure S6H) and increased apoptosis (Figure S6I).

To investigate the function of PGK1 autophosphorylation in brain tumor development, we intracranially injected athymic nude mice with LN229 and U87 cells. Consistent with the effect on cell proliferation, knockout of PTEN and knockin expression

(C) U87 cells (1×10^6) with or without PGK1 Y324F knockin were intracranially injected into athymic nude mice (n = 7 per group). Mice were sacrificed and examined for tumor growth 28 days after injection. Representative H&E-stained brain sections are shown (left panel). Tumor volumes were calculated. The data represent the means ± SDs of 7 mice in each group (right panel). **$p < 0.001$.

(D and E) IHC staining of mouse tumor tissues was performed with antibody against Ki-67 (D) or PGK1 pY324 (E). Representative images are shown. Scale bars, 50 μm (D) or 100 μm (E).

(F) TUNEL analyses of the indicated tumor tissues were performed. Apoptotic cells were stained brown. Scale bar, 50 μm.

(G) Cells from 3 *in situ* brain tumors of each group were isolated and cultured. Glycolytic rate (left panel) and lactate production (right panel) were measured. The data represent the means ± SDs of triplicate experiments.

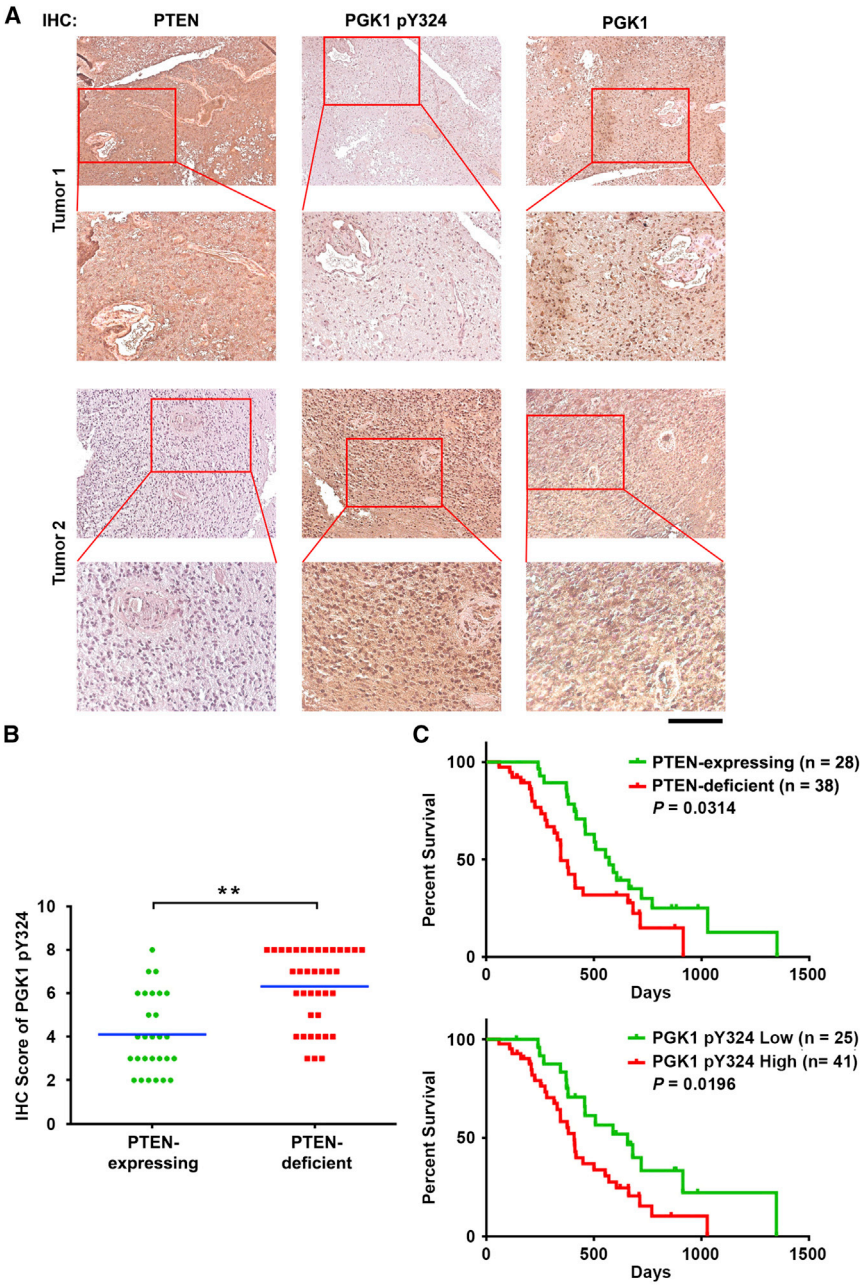

Figure 6. High Levels of PGK1 Autophosphorylation Correlate with Poor Prognosis in GBM Patients

(A) IHC staining of human GBM specimens was performed with the indicated antibodies. Representative images are shown. Scale bar, 100 μm.

(B) Scatterplot of the semiquantitative IHC staining score for PGK1 pY324 in 66 GBM samples is shown. **$p < 0.001$.

(C) Kaplan-Meier plots of the overall survival rates of GBM patients with PTEN-expressing or PTEN-deficient (top panel) and with low (staining score, 0–4) or high (staining score, 5–8) PGK1 pY324 levels (bottom panel). p values were calculated using the log rank test.

of PTEN Y138L in LN229 cells enhanced tumor growth to a varied extent (Figure S6J). We also detected rapid tumor growth in animals injected with parental U87 cells (Figure 5C), which corresponded with high levels of Ki-67 staining (Figures 5D and S6K) and strong PGK1 Y324 phosphorylation (Figure 5E), as detected by a specificity-validated antibody (Figure S6L). In contrast, we detected much smaller tumors (Figures 5C and S6M) with enhanced apoptosis (Figure 5F) in the brains of mice injected with U87 cells expressing the PGK1 Y324F or the PTEN G129E mutant. In addition, cells isolated from tumors expressing PGK1 Y324F had lower glycolytic rates than did those expressing WT PGK1 (Figure 5G). These results indicated that PGK1 autophosphorylation is critical for brain tumorigenesis.

High Levels of PGK1 Autophosphorylation Correlate with Poor Prognosis in GBM Patients

We next analyzed 66 human primary GBM specimens and divided them into WT PTEN-expressing (n = 28) and PTEN-deficient (n = 38) groups on the basis of immunohistochemistry (IHC) staining of PTEN and *PTEN* DNA sequencing analyses (data not shown). IHC staining showed that PTEN expression levels inversely correlated with the phosphorylation levels of PGK1 Y324 (Figure 6A). Quantification of the staining showed that the correlation was significant (Figure 6B). We next compared the survival duration of these patients, all of whom had received standard adjuvant radiotherapy after surgical resection of GBM followed by treatment with an alkylating agent (temozolomide in most cases), with tumor PTEN and PGK1 Y324 phosphorylation levels. The median survival durations were 50.2 and 58.6 weeks for patients whose tumors had no PTEN expression and high PGK1 Y324 phosphorylation levels, respectively, and 78.1 and 92.8 weeks for those whose tumors had PTEN expression and low PGK1 Y324 phosphorylation levels, respectively (Figure 6C). These results support a role for PTEN-dependent PGK1 autophosphorylation in the clinical behavior of human GBM and reveal a correlation between PGK1 autophosphorylation and the clinical aggressiveness of GBM.

DISCUSSION

PGK1, an instrumental ATP-generating enzyme in the glycolytic pathway, is upregulated in many types of human cancers.

However, how PGK1 is posttranslationally regulated to promote glycolysis and tumorigenesis is largely unknown. We showed here that PGK1 is a protein kinase that autophosphorylates at Y324, thereby activating its glycolytic enzymatic activity. In addition to enhancing glycolytic flux, PGK1 Y324 phosphorylation may have a function in accelerating PGK1-mediated DNA replication (Li et al., 2018). PGK1 activity is governed by PTEN protein phosphatase activity, which directly dephosphorylates and inhibits PGK1. Loss of PTEN function, which occurs frequently in tumor cells, resulted in increased PGK1 autophosphorylation, glycolysis, and ATP production and promoted cell proliferation and tumorigenesis.

Thus, we demonstrated for the first time that the protein phosphatase activity of PTEN directly regulates glycolysis by the dephosphorylation and inhibition of PGK1. In addition, we revealed for the first time that PGK1, which is a glycolytic enzyme, acts as a protein kinase to autophosphorylate itself and enhance its activity. That inhibition of PGK1 autophosphorylation largely blocked glycolysis and brain tumor development and that PGK1 autophosphorylation levels predicted GBM patient survival highlight PGK1 as an attractive molecular target for improved cancer prognosis and treatment.

STAR★METHODS

Detailed methods are provided in the online version of this paper and include the following:

SUPPLEMENTAL INFORMATION

Supplemental Information can be found online at https://doi.org/10.1016/j.molcel.2019.08.006.

ACKNOWLEDGMENTS

We thank Dr. David Hawke at MD Anderson Cancer Center for technical assistance. We thank Dr. Hui-Kuan Lin (Wake Forest School of Medicine) for $Pten^{+/+}$ and $Pten^{-/-}$ MEF cells. We thank Dr. Xuejun Jiang (Memorial Sloan Kettering Cancer Center) for the pTRIPZ-PTEN shRNA construct. This work was supported by Start Funding KY103RC20190002 and Science and Technology Development Fund of Nanjing Medical University JX218317201711010 (to X.Q.), NIH grants 1S10OD012304-01 (to P.L.L.) and P30CA016672 (to P.L.L.), and Cancer Prevention and Research Institute of Texas grant RP130397 (to P.L.L.). Z.L. is a Kuangcheng Wang Distinguished Chair.

AUTHOR CONTRIBUTIONS

This study was conceived and designed by Z.L. and X.Q.; X.Q., X.L., Z.S., Y.X., Q.C., D.X., L.T., L.D., Y.Z., and D.Z. performed the experiments; C.Z. and T.J. provided pathology assistance; P.L.L., Y.Y., B.-H.J., and H.L. provided reagents and technical support. Z.L. wrote the paper with comments from all of the authors.

DECLARATION OF INTERESTS

Z.L. owns shares in Signalway Biotechnology (Pearland, TX), which supplied rabbit antibodies that recognize PGK1 pY324. Z.L.'s interest in this company had no bearing on its being chosen to supply these reagents.

Received: September 6, 2018
Revised: June 3, 2019
Accepted: August 2, 2019
Published: September 3, 2019

REFERENCES

Ahmad, S.S., Glatzle, J., Bajaeifer, K., Bühler, S., Lehmann, T., Königsrainer, I., Vollmer, J.P., Sipos, B., Ahmad, S.S., Northoff, H., et al. (2013). Phosphoglycerate kinase 1 as a promoter of metastasis in colon cancer. Int. J. Oncol. *43*, 586–590.

Ai, J., Huang, H., Lv, X., Tang, Z., Chen, M., Chen, T., Duan, W., Sun, H., Li, Q., Tan, R., et al. (2011). FLNA and PGK1 are two potential markers for progression in hepatocellular carcinoma. Cell. Physiol. Biochem. *27*, 207–216.

Bernstein, B.E., and Hol, W.G. (1998). Crystal structures of substrates and products bound to the phosphoglycerate kinase active site reveal the catalytic mechanism. Biochemistry *37*, 4429–4436.

Davidson, L., Maccario, H., Perera, N.M., Yang, X., Spinelli, L., Tibarewal, P., Glancy, B., Gray, A., Weijer, C.J., Downes, C.P., and Leslie, N.R. (2010). Suppression of cellular proliferation and invasion by the concerted lipid and protein phosphatase activities of PTEN. Oncogene *29*, 687–697.

Duan, Z., Lamendola, D.E., Yusuf, R.Z., Penson, R.T., Preffer, F.I., and Seiden, M.V. (2002). Overexpression of human phosphoglycerate kinase 1 (PGK1) induces a multidrug resistance phenotype. Anticancer Res. *22*, 1933–1941.

Fang, D., Hawke, D., Zheng, Y., Xia, Y., Meisenhelder, J., Nika, H., Mills, G.B., Kobayashi, R., Hunter, T., and Lu, Z. (2007). Phosphorylation of beta-catenin by AKT promotes beta-catenin transcriptional activity. J. Biol. Chem. *282*, 11221–11229.

Gu, T., Zhang, Z., Wang, J., Guo, J., Shen, W.H., and Yin, Y. (2011). CREB is a novel nuclear target of PTEN phosphatase. Cancer Res. *71*, 2821–2825.

Humphrey, W., Dalke, A., and Schulten, K. (1996). VMD: visual molecular dynamics. J. Mol. Graph. *14*, 33–38, 27–28.

Hwang, T.L., Liang, Y., Chien, K.Y., and Yu, J.S. (2006). Overexpression and elevated serum levels of phosphoglycerate kinase 1 in pancreatic ductal adenocarcinoma. Proteomics *6*, 2259–2272.

Jiang, Y., Li, X., Yang, W., Hawke, D.H., Zheng, Y., Xia, Y., Aldape, K., Wei, C., Guo, F., Chen, Y., and Lu, Z. (2014). PKM2 regulates chromosome segregation and mitosis progression of tumor cells. Mol. Cell *53*, 75–87.

Kleinstiver, B.P., Pattanayak, V., Prew, M.S., Tsai, S.Q., Nguyen, N.T., Zheng, Z., and Joung, J.K. (2016). High-fidelity CRISPR-Cas9 nucleases with no detectable genome-wide off-target effects. Nature *529*, 490–495.

Lallemand, P., Chaloin, L., Roy, B., Barman, T., Bowler, M.W., and Lionne, C. (2011). Interaction of human 3-phosphoglycerate kinase with its two substrates: is substrate antagonism a kinetic advantage? J. Mol. Biol. *409*, 742–757.

Lane, A.N., and Fan, T.W. (2015). Regulation of mammalian nucleotide metabolism and biosynthesis. Nucleic Acids Res. *43*, 2466–2485.

Lee, J.J., Kim, B.C., Park, M.J., Lee, Y.S., Kim, Y.N., Lee, B.L., and Lee, J.S. (2011). PTEN status switches cell fate between premature senescence and apoptosis in glioma exposed to ionizing radiation. Cell Death Differ. *18*, 666–677.

Lee, J.H., Liu, R., Li, J., Zhang, C., Wang, Y., Cai, Q., Qian, X., Xia, Y., Zheng, Y., Piao, Y., et al. (2017). Stabilization of phosphofructokinase 1 platelet isoform by AKT promotes tumorigenesis. Nat. Commun. *8*, 949.

Li, J., Yen, C., Liaw, D., Podsypanina, K., Bose, S., Wang, S.I., Puc, J., Miliaresis, C., Rodgers, L., McCombie, R., et al. (1997). PTEN, a putative protein tyrosine phosphatase gene mutated in human brain, breast, and prostate cancer. Science *275*, 1943–1947.

Li, X., Jiang, Y., Meisenhelder, J., Yang, W., Hawke, D.H., Zheng, Y., Xia, Y., Aldape, K., He, J., Hunter, T., et al. (2016). Mitochondria-Translocated PGK1 Functions as a Protein Kinase to Coordinate Glycolysis and the TCA Cycle in Tumorigenesis. Mol. Cell *61*, 705–719.

Li, X., Qian, X., Jiang, H., Xia, Y., Zheng, Y., Li, J., Huang, B.J., Fang, J., Qian, C.N., Jiang, T., et al. (2018). Nuclear PGK1 Alleviates ADP-Dependent Inhibition of CDC7 to Promote DNA Replication. Mol. Cell *72*, 650–660.e8.

Liaw, D., Marsh, D.J., Li, J., Dahia, P.L., Wang, S.I., Zheng, Z., Bose, S., Call, K.M., Tsou, H.C., Peacocke, M., et al. (1997). Germline mutations of the PTEN gene in Cowden disease, an inherited breast and thyroid cancer syndrome. Nat. Genet. *16*, 64–67.

Lu, Z., and Hunter, T. (2009). Degradation of activated protein kinases by ubiquitination. Annu. Rev. Biochem. *78*, 435–475.

Lu, Z., Liu, D., Hornia, A., Devonish, W., Pagano, M., and Foster, D.A. (1998). Activation of protein kinase C triggers its ubiquitination and degradation. Mol. Cell. Biol. *18*, 839–845.

Maehama, T., and Dixon, J.E. (1998). The tumor suppressor, PTEN/MMAC1, dephosphorylates the lipid second messenger, phosphatidylinositol 3,4,5-trisphosphate. J. Biol. Chem. *273*, 13375–13378.

Myers, M.P., Stolarov, J.P., Eng, C., Li, J., Wang, S.I., Wigler, M.H., Parsons, R., and Tonks, N.K. (1997). P-TEN, the tumor suppressor from human chromosome 10q23, is a dual-specificity phosphatase. Proc. Natl. Acad. Sci. USA *94*, 9052–9057.

Myers, M.P., Pass, I., Batty, I.H., Van der Kaay, J., Stolarov, J.P., Hemmings, B.A., Wigler, M.H., Downes, C.P., and Tonks, N.K. (1998). The lipid phosphatase activity of PTEN is critical for its tumor supressor function. Proc. Natl. Acad. Sci. USA *95*, 13513–13518.

Qian, X., Li, X., Cai, Q., Zhang, C., Yu, Q., Jiang, Y., Lee, J.H., Hawke, D., Wang, Y., Xia, Y., et al. (2017a). Phosphoglycerate Kinase 1 Phosphorylates Beclin1 to Induce Autophagy. Mol. Cell *65*, 917–931.e6.

Qian, X., Li, X., and Lu, Z. (2017b). Protein kinase activity of the glycolytic enzyme PGK1 regulates autophagy to promote tumorigenesis. Autophagy *13*, 1246–1247.

Ran, F.A., Hsu, P.D., Wright, J., Agarwala, V., Scott, D.A., and Zhang, F. (2013). Genome engineering using the CRISPR-Cas9 system. Nat. Protoc. *8*, 2281–2308.

Shi, Y., Wang, J., Chandarlapaty, S., Cross, J., Thompson, C., Rosen, N., and Jiang, X. (2014). PTEN is a protein tyrosine phosphatase for IRS1. Nat. Struct. Mol. Biol. *21*, 522–527.

Song, M.S., Salmena, L., and Pandolfi, P.P. (2012). The functions and regulation of the PTEN tumour suppressor. Nat. Rev. Mol. Cell Biol. *13*, 283–296.

Stambolic, V., Suzuki, A., de la Pompa, J.L., Brothers, G.M., Mirtsos, C., Sasaki, T., Ruland, J., Penninger, J.M., Siderovski, D.P., and Mak, T.W. (1998). Negative regulation of PKB/Akt-dependent cell survival by the tumor suppressor PTEN. Cell *95*, 29–39.

Steck, P.A., Pershouse, M.A., Jasser, S.A., Yung, W.K., Lin, H., Ligon, A.H., Langford, L.A., Baumgard, M.L., Hattier, T., Davis, T., et al. (1997). Identification of a candidate tumour suppressor gene, MMAC1, at chromosome 10q23.3 that is mutated in multiple advanced cancers. Nat. Genet. *15*, 356–362.

Sun, H., Lesche, R., Li, D.M., Liliental, J., Zhang, H., Gao, J., Gavrilova, N., Mueller, B., Liu, X., and Wu, H. (1999). PTEN modulates cell cycle progression and cell survival by regulating phosphatidylinositol 3,4,5,-trisphosphate and Akt/protein kinase B signaling pathway. Proc. Natl. Acad. Sci. USA *96*, 6199–6204.

Tamura, M., Gu, J., Matsumoto, K., Aota, S., Parsons, R., and Yamada, K.M. (1998). Inhibition of cell migration, spreading, and focal adhesions by tumor suppressor PTEN. Science *280*, 1614–1617.

Tiganis, T., and Bennett, A.M. (2007). Protein tyrosine phosphatase function: the substrate perspective. Biochem. J. *402*, 1–15.

Vander Heiden, M.G., Cantley, L.C., and Thompson, C.B. (2009). Understanding the Warburg effect: the metabolic requirements of cell proliferation. Science *324*, 1029–1033.

Wang, J., Han, F., Wu, J., Lee, S.W., Chan, C.H., Wu, C.Y., Yang, W.L., Gao, Y., Zhang, X., Jeong, Y.S., et al. (2011). The role of Skp2 in hematopoietic stem cell quiescence, pool size, and self-renewal. Blood *118*, 5429–5438.

Wang, S., Jiang, B., Zhang, T., Liu, L., Wang, Y., Wang, Y., Chen, X., Lin, H., Zhou, L., Xia, Y., et al. (2015). Insulin and mTOR Pathway Regulate HDAC3-Mediated Deacetylation and Activation of PGK1. PLoS Biol. *13*, e1002243.

Wick, W., Furnari, F.B., Naumann, U., Cavenee, W.K., and Weller, M. (1999). PTEN gene transfer in human malignant glioma: sensitization to irradiation and CD95L-induced apoptosis. Oncogene *18*, 3936–3943.

Wozniak, D.J., Kajdacsy-Balla, A., Macias, V., Ball-Kell, S., Zenner, M.L., Bie, W., and Tyner, A.L. (2017). PTEN is a protein phosphatase that targets active PTK6 and inhibits PTK6 oncogenic signaling in prostate cancer. Nat. Commun. *8*, 1508.

Xia, Y., Wang, J., Liu, T.J., Yung, W.K., Hunter, T., and Lu, Z. (2007). c-Jun downregulation by HDAC3-dependent transcriptional repression promotes osmotic stress-induced cell apoptosis. Mol. Cell *25*, 219–232.

Yan, H., Yang, K., Xiao, H., Zou, Y.J., Zhang, W.B., and Liu, H.Y. (2012). Over-expression of cofilin-1 and phosphoglycerate kinase 1 in astrocytomas involved in pathogenesis of radioresistance. CNS Neurosci. Ther. *18*, 729–736.

Yang, W., and Lu, Z. (2013). Regulation and function of pyruvate kinase M2 in cancer. Cancer Lett. *339*, 153–158.

Yang, W., and Lu, Z. (2015). Pyruvate kinase M2 at a glance. J. Cell Sci. *128*, 1655–1660.

Yang, W., Xia, Y., Ji, H., Zheng, Y., Liang, J., Huang, W., Gao, X., Aldape, K., and Lu, Z. (2011). Nuclear PKM2 regulates β-catenin transactivation upon EGFR activation. Nature *480*, 118–122.

Zerrad, L., Merli, A., Schröder, G.F., Varga, A., Gráczer, É., Pernot, P., Round, A., Vas, M., and Bowler, M.W. (2011). A spring-loaded release mechanism regulates domain movement and catalysis in phosphoglycerate kinase. J. Biol. Chem. *286*, 14040–14048.

Zhang, D., Tai, L.K., Wong, L.L., Chiu, L.L., Sethi, S.K., and Koay, E.S. (2005). Proteomic study reveals that proteins involved in metabolic and detoxification pathways are highly expressed in HER-2/neu-positive breast cancer. Mol. Cell. Proteomics *4*, 1686–1696.

Zhang, S., Huang, W.C., Li, P., Guo, H., Poh, S.B., Brady, S.W., Xiong, Y., Tseng, L.M., Li, S.H., Ding, Z., et al. (2011). Combating trastuzumab resistance by targeting SRC, a common node downstream of multiple resistance pathways. Nat. Med. *17*, 461–469.

Zheng, Y., Xia, Y., Hawke, D., Halle, M., Tremblay, M.L., Gao, X., Zhou, X.Z., Aldape, K., Cobb, M.H., Xie, K., et al. (2009). FAK phosphorylation by ERK primes ras-induced tyrosine dephosphorylation of FAK mediated by PIN1 and PTP-PEST. Mol. Cell *35*, 11–25.

Zieker, D., Königsrainer, I., Tritschler, I., Löffler, M., Beckert, S., Traub, F., Nieselt, K., Bühler, S., Weller, M., Gaedcke, J., et al. (2010). Phosphoglycerate kinase 1 a promoting enzyme for peritoneal dissemination in gastric cancer. Int. J. Cancer *126*, 1513–1520.

STAR★METHODS

KEY RESOURCES TABLE

REAGENT or RESOURCE	SOURCE	IDENTIFIER
Antibodies		
Rabbit polyclonal antibody anti-PGK1 pY324	Signalway Biotechnology	N/A
Rabbit polyclonal antibody anti-PGK1 pS203	Li et al., 2016	N/A
Rabbit polyclonal antibody anti-Beclin1 pS30	Qian et al., 2017a	N/A
Rabbit polyclonal antibody anti-HA	Signalway Biotechnology	Cat# 35534; RRID: AB_2688030
Rabbit polyclonal antibody anti-PGK1	Abcam	Cat# ab38007; RRID: AB_2161220
Rabbit polyclonal antibody anti-MCM2	Abcam	Cat# ab4461; RRID: AB_304470
Mouse monoclonal antibody anti-MCM2 pS53	Abcam	Cat# ab109133; RRID: AB_10863901
Mouse monoclonal antibody anti-CDC7	Abcam	Cat# ab10535; RRID: AB_297276
Rabbit monoclonal antibody anti-PTEN	Cell Signaling Technology	Cat# 9559; RRID: AB_390810
Rabbit polyclonal antibody anti-AKT	Cell Signaling Technology	Cat# 4685; RRID: AB_10698888
Rabbit monoclonal antibody anti-AKT pT308	Cell Signaling Technology	Cat# 9266; RRID: AB_689801
Rabbit monoclonal antibody anti-AKT pS473	Cell Signaling Technology	Cat# 4060; RRID: AB_2315049
Rabbit polyclonal antibody anti-p70S6K	Cell Signaling Technology	Cat# 9202; RRID: AB_10695156
Mouse monoclonal antibody anti-p70S6K pT389	Cell Signaling Technology	Cat# 9206S; RRID: AB_331790
Rabbit monoclonal antibody anti-PARP	Cell Signaling Technology	Cat# 9532; RRID: AB_659884
Mouse monoclonal antibody anti-pTyr	Santa Cruz Biotechnology	Cat# sc-7020; RRID: AB_628123
Mouse monoclonal antibody anti-GST	Santa Cruz Biotechnology	Cat# sc-138; RRID: AB_627677
Mouse monoclonal antibody anti- α Tubulin	Santa Cruz Biotechnology	Cat# sc-5286; RRID: AB_628411
Mouse monoclonal antibody anti-Flag	Sigma-Aldrich	Cat# F3165; RRID: AB_259529
Mouse monoclonal antibody anti-His	Sigma-Aldrich	Cat# SAB2702219
Bacterial and Virus Strains		
BL21(DE3)	EMD Millipore	Cat# 71401-3
TOP10	ThermoFisher Scientific	Cat# C404010
Biological Samples		
Human GBM specimens	The Chinese Glioma Genome Atlas	www.cgga.org.cn
Chemicals, Peptides, and Recombinant Proteins		
EGF	Sigma-Aldrich	Cat# E9644
Phosphoenolpyruvate (PEP)	Sigma-Aldrich	Cat# P7002
Pyruvate	Sigma-Aldrich	Cat# P5280
doxycycline	Sigma-Aldrich	Cat# D3447
D-3-phosphoglycerate (3-PG)	Sigma-Aldrich	Cat# P8877
D-glyceraldehyde 3-phosphate (GAP)	Sigma-Aldrich	Cat# 39705
IPTG	Sigma-Aldrich	Cat# I6758
ADP	Sigma-Aldrich	Cat# A2754
ATP	Sigma-Aldrich	Cat# A6419
NAD^+	Sigma-Aldrich	Cat# N6522
NADH	Sigma-Aldrich	Cat# N1161
DAPI	Sigma-Aldrich	Cat# D9542
Active glyceraldehyde 3-phosphate dehydrogenase (GAPDH)	Sigma-Aldrich	Cat# SRE0024
Streptavidin-conjugated agarose beads	Sigma-Aldrich	Cat#16-126
3 × Flag peptide	ThermoFisher Scientific	Cat# A36805
c-Myc peptide	ThermoFisher Scientific	Cat# 20170

(*Continued on next page*)

Continued

REAGENT or RESOURCE	SOURCE	IDENTIFIER
HA peptide	ThermoFisher Scientific	Cat# 26184
Anti-HA Magnetic Beads	ThermoFisher Scientific	Cat# 88837
Anti-DYKDDDDK Tag (L5) Affinity Gel	BioLegend	Cat# 651503
Anti-c-Myc Tag (9E10) Affinity Gel	BioLegend	Cat# 658502
Ni-NTA His•Bind® Resin	EMD Millipore	Cat# 70666
Phosphatidylinositol 3,4,5-trisphosphate diC8 (diC8-PI [3,4,5]P3)	Echelon Biosciences, Inc.	Cat# P-3908
[γ-^{32}P]-ATP	MP Biochemicals	Cat# 0135001
[8-^{14}C]-ADP	Perkin Elmer	Cat# 0113004
D-[5-^{3}H]-glucose	Perkin Elmer	Cat# NET53100
$^{13}C_6$-glucose	Cambridge Isotope Laboratories, Inc.	Cat# CLM-1396
$^{13}C_5$-glutamine	Cambridge Isotope Laboratories, Inc.	Cat# CLM-1822
LY294002	Selleck Chemicals	Cat# S1105
MK-2206	Selleck Chemicals	Cat# S1078
Critical Commercial Assays		
ATP Colorimetric/Fluorometric Assay Kit	BioVision	Cat# K354-100
L-Lactate Assay Kit II	Eton Bioscience	Cat# 120005
QuikChange site-directed mutagenesis kit	Agilent Technologies	Cat# 200524
Tumor Dissociation Kit, mouse	Miltenyi Biotec Inc.	Cat# 130-096-730
VECTASTAIN Elite ABC HRP Kit	Vector Laboratories	Cat# PK-6101
Liquid DAB+ Substrate Chromogen System	Dako	Cat# K3468
Seahorse XF Analyzer	Agilent Technologies	N/A
Malachite Green Assay Kit	Echelon Biosciences Inc	Cat# K-1500
SensoLyte FDP Protein Phosphatase Assay Kit	AnaSpec Co	Cat# AS-71100
DeadEnd Colorimetric TUNEL System	Promega	Cat# G7360
Deposited Data		
Raw Data	This paper, Mendeley Data	https://data.mendeley.com/datasets/3s8ny9vh85/draft?a=2b486ba9-a277-45a6-bfb7-546f806deb7a
Experimental Models: Cell Lines		
Human: U87	ATCC	Cat# HTB-14
Human: U251	Sigma-Aldrich	Cat# 09063001
Human: A172	ATCC	Cat# CRL-1620
Human: LN229	ATCC	Cat# CRL-2611
Human: LN18	ATCC	Cat# CRL-2610
Human: HEK293T	ATCC	Cat# CRL-11268
Mouse: Pten$^{+/+}$ MEFs	Wang et al., 2011	N/A
Mouse: Pten$^{-/-}$ MEFs	Wang et al., 2011	N/A
Experimental Models: Organisms/Strains		
Mouse: BALB/c nude	The University of Texas MD Anderson Cancer Center	N/A
Mouse: BALB/c nude	Model Animal Research Center of Nanjing University	N/A
Oligonucleotides		
PGK1 pY324 peptide (318-PESSKK-pY-AEAVTR-330)	This paper, synthesized by Selleck Chemicals	N/A
acidic standard PTEN substrate peptide poly-(EY) (RRREEEpYEEE)	This paper, synthesized by Selleck Chemicals	N/A
Primers used in this paper, see Table S3	This paper	N/A

(*Continued on next page*)

Continued

REAGENT or RESOURCE	SOURCE	IDENTIFIER
Recombinant DNA		
pGIPZ PTEN shRNA	Dharmacon	V2LHS_92314
pcDNA3.1 HA-PTEN WT	This paper	N/A
pcDNA3.1 HA-PTEN C124S	This paper	N/A
pcDNA3.1 HA-PTEN G129E	This paper	N/A
pcDNA3.1 HA-PTEN Y138L	This paper	N/A
pcDNA3.1 Flag-PTEN WT	This paper	N/A
pcDNA3.1 Flag-PTEN C124S	This paper	N/A
pcDNA3.1 Flag-PTEN D92A	This paper	N/A
pColdI PTEN WT	This paper	N/A
pColdI PTEN C124S	This paper	N/A
pColdI PTEN G129E	This paper	N/A
pColdI PTEN Y138L	This paper	N/A
pGIPZ PGK1 shRNA	Qian et al., 2017a	N/A
pcDNA3.1 HA-PGK1 WT	Qian et al., 2017a	N/A
pcDNA3.1 HA-PGK1 T378P	This paper	N/A
pcDNA3.1 Flag-PGK1 WT	This paper	N/A
pcDNA3.1 Flag-PGK1 Y324F	This paper	N/A
pcDNA3.1 Flag-PGK1 S203A	This paper	N/A
pcDNA3.1 Flag-PGK1 S256A	This paper	N/A
pcDNA6-SFB PGK1 WT	This paper	N/A
pcDNA6-SFB PGK1 Y324F	This paper	N/A
pcDNA6-SFB PGK1 T378P	This paper	N/A
PGEX-4T-1 PGK1 WT	This paper	N/A
PGEX-4T-1 PGK1 T378P	This paper	N/A
PGEX-4T-1 PGK1 Y324F/T378P	This paper	N/A
pColdI PGK1 WT	This paper	N/A
pColdI PGK1 Y324F	This paper	N/A
pColdI PGK1 T378P	This paper	N/A
pcDNA3.1 Flag-Beclin1 WT	Qian et al., 2017a	N/A
pcDNA3.1 Flag-Beclin1 S30A	Qian et al., 2017a	N/A
PX458	Ran et al., 2013	Addgene #48138
HA-Myr-AKT	Addgene	Cat# 10841
Flag-PTP-PEST	Zheng et al., 2009	N/A
HA-RPTPa	Zheng et al., 2009	N/A
Myc-SHP1	Zheng et al., 2009	N/A
Myc-SHP2	Zheng et al., 2009	N/A
Software and Algorithms		
Protein Data Bank	RCSB PDB	www.rcsb.org
Discover Studio Visualizer	Accelrys	accelrys.com
UCSF Chimera	UCSF	www.cgl.ucsf.edu/chimera
Amber 16 Molecular Dynamics package	UCSF	ambermd.org
PyMOL	Schrödinger, LLC	https://pymol.org/2/
SeeSAR	BioSolveIT GmbH	https://www.biosolveit.de/SeeSAR
CRISPR Design tool	Zhang Lab	https://zlab.bio/guide-design-resources

LEAD CONTACT AND MATERIALS AVAILABILITY

Further information and requests for resources and reagents should be directed to and will be fulfilled by the Lead Contact, Zhimin Lu (zhiminlu@zju.edu.cn).

EXPERIMENTAL MODEL AND SUBJECT DETAILS

Mice

Cells (1×10^6) were suspended in 5 μL of DMEM and intracranially injected into 4-week-old female athymic nude mice as described previously (Yang et al., 2011). Mice were sacrificed 28 days after injection. Brains were harvested, fixed in 4% formaldehyde, and embedded in paraffin. Tumor formation was determined by hematoxylin and eosin staining. Tumor volume was calculated using the formula $0.5 \times \text{length}^2 \times \text{width}$. The use of animals was approved by the Institutional Animal Care and Use Committee (IACUC) of The University of Texas MD Anderson Cancer Center and by Nanjing Medical University.

For isolating tumor cells from mouse brains, mice were sacrificed 21 days after injection. Tumor cell isolation was performed by using a Tumor Dissociation Kit (Miltenyi Biotec Inc., Auburn, CA) according to the manufacturer's instructions.

Human subjects and immunohistochemical staining

The human GBM samples and clinical information were obtained from the Chinese Glioma Genome Atlas (CGGA, http://www.cgga.org.cn). This study included 66 GBM samples with PTEN status determined on the basis of IHC staining and sequencing; 28 samples were PTEN-expressing and 38 were PTEN-deficient. Sections of paraffin-embedded human GBM tissues were stained with antibodies against PGK1 pY324 and PTEN. The staining of the tissues was then quantitatively scored according to the percentage of positive cells and staining intensity as described previously (Qian et al., 2017a). The following proportion scores were assigned to the sections: 0 if 0% of tumor cells exhibited positive staining, 1 for 0 to 1% positive cells, 2 for 2% to 10% positive cells, 3 for 11% to 30% positive cells, 4 for 31% to 70% positive cells, and 5 for 71% to 100% positive cells. In addition, the staining intensity was scored on a scale of 0-3: 0, negative; 1, weak; 2, moderate; and 3, strong. The proportion and intensity scores were then added to obtain a total score ranging from 0 to 8 as described previously (Qian et al., 2017a). Scores were compared with overall survival duration, defined as the time from date of diagnosis to death or last known follow-up examination. The use of human GBM samples and the clinical parameters were approved by the Institutional Review Board at Capital Medical University in Beijing, China.

Cell culture and transfection

U87, U251, A172, D54, LN229, and LN18 human GBM cells and human embryonic kidney 293T cells were maintained in Dulbecco's modified Eagle's medium (DMEM) supplemented with 10% bovine calf serum (BCS; Hyclone, Logan, UT). Immortalized $Pten^{+/+}$ and $Pten^{-/-}$ MEFs were kindly provided by Dr. Hui-Kun Lin (Wake Forest School of Medicine) (Wang et al., 2011) and maintained in DMEM supplemented with 10% fetal bovine serum (Hyclone, Logan, UT).

Cells were plated at a density of 4×10^5 per 60-mm dish or 1×10^5 per well of a 6-well plate 18 h before transfection. The transfection procedure was performed as previously described (Xia et al., 2007).

METHOD DETAILS

Materials

Rabbit polyclonal antibody against PGK1 Y324 phosphorylation was produced by Signalway Biotechnology (Pearland, TX). Rabbit polyclonal antibody against HA was also obtained from Signalway Biotechnology. Rabbit polyclonal antibodies against PGK1 pS203 and Beclin1 pS30 were reported before (Li et al., 2016; Qian et al., 2017a). Rabbit polyclonal antibodies recognizing PGK1 and MCM2 and mouse monoclonal antibodies against CDC7 and MCM2 pS53 were obtained from Abcam (Cambridge, MA). Antibodies recognizing PTEN, AKT, AKT pT308, AKT pS473, p70S6K pT389, p70S6K, and PARP were purchased from Cell Signaling Technology (Danvers, MA). Antibodies against p-Tyr, GST, α-tubulin, normal rabbit IgG and normal mouse IgG were from Santa Cruz Biotechnology (Santa Cruz, CA). Mouse monoclonal antibodies against Flag and His, active glyceraldehyde 3-phosphate dehydrogenase (GAPDH) recombinant protein, EGF, sodium orthovanadate, PEP, Triton X-100, doxycycline, 3-PG, glyceraldehyde 3-phosphate (GAP), ADP, ATP, NAD^+ and NADH were purchased from Sigma (St. Louis, MO). Anti-DYKDDDDK (Flag) tag affinity gel and anti-c-Myc tag (9E10) affinity gel were purchased from BioLegend (San Diego, CA). 3 × Flag peptide, c-Myc peptide, HA peptide, anti-HA magnetic beads and streptavidin beads were purchased from ThermoFisher Scientific (Pittsburgh, PA). Ni-NTA His•Bind Resin was purchased from EMD Millipore (Billerica, MA). Phosphatidylinositol 3,4,5-trisphosphate diC8 (diC8-PI[3,4,5]P3) was obtained from Echelon Biosciences, Inc. (Salt Lake City, UT). [γ-^{32}P]-ATP was purchased from MP Biochemicals (Santa Ana, CA). [8-^{14}C]-ADP and D-[5-^{3}H]-glucose were purchased from Perkin Elmer (Waltham, MA). $^{13}C_6$-glucose and $^{13}C_5$-glutamine were purchased from Cambridge Isotope Laboratories, Inc. (Tewksbury, MA). LY294002 was purchased from LC Laboratories (Woburn, MA). MK-2206 was purchased from Selleck Chemicals (Houston, TX).

DNA constructs and mutagenesis

Polymerase chain reaction (PCR)-amplified human PGK1 and PTEN were cloned into pcDNA3.1/hygro(+)-Flag, pcDNA3-HA, pcDNA6/SFB, pColdI or pGEX-4T-1 vectors. PGK1 S203A, S256A, Y324F, and T378P mutants, and PTEN C124S, G129E, and Y138L mutants were generated using a QuikChange site-directed mutagenesis kit (Stratagene, La Jolla, CA). Generation of HA-Myr-AKT, Flag-PTP-PEST, HA-RPTPa, Myc-SHP1 and Myc-SHP2 constructs was described previously (Lee et al., 2017; Zheng et al., 2009). shRNA-resistant (r) PGK1 or rPTEN was made by introducing nonsense mutations in shRNA-targeting sites as described previously (Yang et al., 2011). pGIPZ PGK1 shRNA was generated as previously described (Li et al., 2016). pGIPZ PTEN shRNA (V2LHS_92314) was purchased from Dharmacon (Lafayette, CO).

Glucose glycolytic rate assay

The glycolytic rate was determined by measuring the conversion of D-[5-^{3}H]-glucose to ^3H_2O as described previously (Li et al., 2016). Briefly, 1×10^6 cells were washed with PBS and then incubated in 2 mL of Krebs buffer (126 mM NaCl, 2.5 mM KCl, 25 mM $NaHCO_3$, 1.2 mM NaH_2PO_4, 1.2 mM $MgCl_2$, 2.5 mM $CaCl_2$) without glucose at 37°C for 30 min. The buffer was then replaced with 2 mL of Krebs buffer containing 5.5 mM glucose spiked with 10 μCi of 5-^{3}H-glucose (0.5 μM). After incubation at 37°C for 1 h, 50 μL aliquots of Krebs buffer were transferred to uncapped PCR tubes containing 50 μL of 0.2 N HCl, which were then placed into Eppendorf tubes containing 0.5 mL H_2O to diffuse ^3H_2O into unlabeled water. The tubes were sealed, and diffusion was allowed to proceed at 37°C for a minimum of 24 h. The amount of diffused ^3H_2O was determined by scintillation counting.

Measurement of lactate production

Cells were seeded and cultured with nonserum DMEM for 20 h. The culture medium was collected to measure the lactate concentration using a lactate assay kit (Eton Bioscience, Inc., San Diego, CA). Lactate production was normalized to cell numbers.

Measurement of ATP concentration

Cells (1×10^6) were seeded and maintained in DMEM with 10% BCS overnight. These cells were then lysed in 100 μL ATP assay buffer. Samples were deproteinized by using 10-kDa cut-through spin columns (Millipore). ATP levels were determined using an ATP Assay Kit (BioVision, Milpitas, CA) and normalized to the amount of protein.

Immunoprecipitation and immunoblotting analysis

Proteins were extracted with a modified buffer, and immunoprecipitation and immunoblotting were performed with the corresponding antibodies as described previously (Lu et al., 1998).

Purification of recombinant proteins

Recombinant proteins were expressed in the BL21 bacterial strain and purified as described previously (Xia et al., 2007). Briefly, the bacteria were cultured in 250 mL lysogeny broth (LB) medium until OD reached 0.6. The protein expression was induced with 0.5 mM isopropyl β-D-1-thiogalactopyranoside (IPTG) overnight at 16°C for $(His)_6$-tagged proteins or at 30°C for GST-tagged proteins. For $(His)_6$-tagged proteins, cell lysates were loaded onto an Ni-NTA column (GE Healthcare Life Sciences, Pittsburgh, PA), then washed with 5 column-volumes of 20 mM imidazole and subsequently eluted with 250 mM imidazole. For GST-tagged proteins, cell lysates were loaded onto a GSTrap HP column (GE Healthcare Life Sciences), then washed with 5 column-volumes of PBS and subsequently eluted with 10 mM reduced glutathione. Proteins were then desalted by washing with PBS using 10-kDa cut-through spin columns.

Streptavidin and His pull-down assay

Streptavidin or Ni-NTA agarose beads were incubated with cell lysates or purified proteins overnight. The beads were then washed with lysate buffer 5 times and subjected to immunoblotting analysis.

Measurement of PGK1 activity

PGK1 catalyzes the reversible phosphotransfer reaction from 1,3-biphosphoglycerate (1,3-BPG) to ADP, leading to the generation of 3-PG and ATP. The measurement of PGK1 activity using ADP as a substrate (the forward reaction) was performed by incubating PGK1 protein (10 ng) in 100 μL reaction buffer (20 mM Tris, 100 mM NaCl, 0.1 mM $MgSO_4$, 10 mM Na_2HPO_4, 2 mM dithiothreitol [DTT] at pH 8.6, 1.6 mM GAP, 0.2 mM NAD, 1 mM ADP and 10 U GAPDH). The measurement of PGK1 activity using ATP as a substrate (the reverse reaction) was performed by incubating PGK1 protein (10 ng) in 100 μL reaction buffer (50 mM Tris-HCl [pH 7.5], 5 mM $MgCl_2$, 5 mM ATP, 0.2 mM NADH, 10 mM 3-PG, and 10 U GAPDH). The reaction was allowed to take place at 25°C in a 96-well plate and read at 339 nm in kinetic mode for 5 min using CLARIOstar microplate reader (BMG Labtech).

In vitro kinase assay

The kinase reaction was performed as described previously (Fang et al., 2007). In brief, recombinant WT PGK1 or PGK1 mutant (200 ng) was incubated in 25 μL kinase buffer (50 mM Tris-HCl [pH 7.5], 100 mM KCl, 50 mM $MgCl_2$, 50 mM $MnCl_2$, 1 mM

Na_3VO_4, 1 mM DTT, 5% glycerol, 0.5 mM ATP, and 10 μCi [γ-^{32}P]-ATP) at 25°C for 1 h. The reaction was terminated by adding sodium dodecyl sulfate-polyacrylamide gel electrophoresis (SDS-PAGE) loading buffer and heated at 100°C for 5 min. The reaction mixture was then subjected to SDS-PAGE analysis.

Determining kinetic parameters of PGK1

Kinetic parameters were assayed by using various concentrations of 3-PG and ATP. Purified recombinant PGK1 protein (100 ng) was incubated in 100 μL reaction buffer (50 mM Tris-HCl [pH 7.5], 5 mM $MgCl_2$, 0.2 mM NADH, and 10 U GAPDH). For measuring the kinetic parameters of ATP, the 3-PG concentration was 5 mM; for measuring the kinetic parameters of 3-PG, the ATP concentration was 5 mM. The reaction was incubated at 25°C in a 96-well plate and read at 339 nm in kinetic mode for 5 min. The reaction velocity (*V*) was obtained by measuring the product concentration as a function of time. To measure the *K*m of ATP for PGK1 Y324 phosphorylation, purified recombinant PGK1 protein (100 ng) was incubated 25 μL kinase buffer with different concentration of ATP for 1 min, followed by immunoblotting analyses. Intensities of PGK1 Y324 phosphorylation levels were determined by ImageJ. K_m and V_{max} were calculated from a plot of 1/*V* versus 1/[substrate] according to the Lineweaver-Burke plot model.

Mass spectrometry analysis

Immunoprecipitated Flag-PTEN C124S-associated proteins or *in vitro* phosphorylated PGK1 proteins were digested and analyzed by LC-MS/MS on an Orbitrap Elite mass spectrometer (ThermoFisher Scientific), as described previously (Jiang et al., 2014).

Analysis of glycolytic intermediate metabolites by LC/MS-MS

Approximately 80% confluent cells were seeded in 10-cm dishes in triplicate. For glucose labeling, cells were washed with glucose-free DMEM medium (11966025, ThermoFisher) and incubated in fresh medium containing $^{13}C_6$-glucose (10 mM) for 30 min. For glutamine labeling, cells were washed with glucose/glutamine-free DMEM (A1443001, GIBCO) and incubated in fresh medium containing 5 mM glucose and 4 mM $^{13}C_5$-glutamine for 6 h. The cells were then quickly washed with ice-cold PBS and flushed with Milli-Q water to remove extra medium components. Metabolites were extracted using 90/9/1 (v/v/v) acetonitrile/water/formic acid. Samples were centrifuged at 17,000 g for 5 min at 4°C, and supernatants were transferred to clean tubes, followed by evaporation to dryness using nitrogen. Samples were reconstituted in deionized water, and then 10 μL was injected into a Thermo Scientific Dionex ICS-5000+ capillary ion chromatography (IC) system containing a Thermo IonPac AS11 4 μm, 250 mm × 2 mm column. The IC flow rate was 360 μl/min (at 30°C), and the gradient conditions were as follows: initial 1 mM KOH, then increased to 35 mM at 25 min, then to 99 mM at 39 min, then held at 99 mM for 10 min. The total run time was 50 min. To assist the desolvation and improve sensitivity, methanol was delivered by an external pump and combined with the eluent via a low dead volume mixing tee. Data were acquired using a Thermo Orbitrap Fusion Tribrid mass spectrometer in electrospray ionization (ESI)-negative mode. The raw data files were imported to Thermo TraceFinder software for final analysis.

Measurement of oxygen consumption rate (OCR)

The extracellular oxygen consumption was determined by OCRs using the Seahorse XF96 extracellular flux analyzer (Seahorse Bioscience) as described before (Li et al., 2016).

Cell proliferation assay

4×10^4 cells were seeded in a 6-well plate and maintained in DMEM with 10% BCS for different periods of time. The cells were trypsinized and counted.

PTEN phosphatase assay

A PTEN phosphatase assay was conducted as described previously (Zhang et al., 2011). PGK1 pY324 peptide (318-PESSKK-pY-AEAVTR-330) synthesized by SelleckChem (Houston, TX) and acidic standard PTEN substrate peptide poly-(EY) (RRREEEpYEEE) synthesized by GenScript (Piscataway, NJ) were dissolved in phosphate-free water to a final concentration of 1 mM. diC8-PI(3,4,5)P3 was used as a positive control for recombinant PTEN protein activity. Purified WT His-PTEN, His-PTEN C124S or His-PTEN G129 mutant proteins (300 ng) were incubated with 100 μM PGK1 pY324 peptide, 100 μM poly-(EY) peptide or 100 μM diC8-PI(3,4,5)P3 in 25 μL phosphatase reaction buffer (25 mM Tris-HCl [pH 7.4], 140 mM NaCl and 10 mM DTT) at 37°C for 30 min. The phosphate released from the substrate was measured using a Malachite Green Assay Kit (Echelon Biosciences Inc, Salt Lake City, UT).

To measure the kinetic parameters of PTEN, 500 ng purified His-PTEN was incubated with various concentrations of PGK1 pY324 peptide or poly-(EY) peptide in 100 μL phosphatase reaction buffer at 37°C for 30 min. The reaction velocity (*V*) was obtained by measuring the phosphate released from the substrate as a function of time. K_m and K_{cat} were calculated from a plot of 1/*V* versus 1/[*substrate*] according to the Lineweaver-Burke plot model.

FDP protein phosphatase assay

Plasmids expressing Flag-PTP-PEST, HA-RPTPα, Myc-SHP1 and Myc-SHP2 were separately transfected into 293T cells. Cell lysates were prepared in Chaps buffer consisting of 10 mM HEPES (pH 7.5), 1% Chaps, 150 mM NaCl, 1 mM DTT, 0.5 mM

ethylenediaminetetraacetic acid (EDTA), 0.1 mM phenylmethylsulfonyl fluoride, 12 mg/ml leupeptin and 20 μg/ml aprotinin. These phosphatases were immunoprecipitated by their corresponding tag antibodies, and their activity toward 3,6-fluorescein diphosphate (FDP) was examined using a SensoLyte FDP Protein Phosphatase Assay Kit *Fluorimetric* (AnaSpec Co., San Jose, CA).

ADP binding assay

Ni-NTA agarose bead-bound His-PGK1 protein was incubated with 2 mM ADP spiked with 4 μCi [8-^{14}C]-ADP at 25°C for 30 min, then quickly washed twice with kinase buffer. The protein-bound radioactivity was detected by scintillation counting.

Molecular dynamic simulation

The fully closed (PDB: 2Y3I) and open (PDB: 1VJD) conformations of PGK1 structures were retrieved from the Protein Data Bank (www.rcsb.org/). Y324-phosphorylated PGK1 was constructed using the ''residue mutate'' option in Discover Studio Visualizer (https://www.3dsbiovia.com/). All nonstandard residues except ATP were removed before simulation. Both nonphosphorylated and Y324-phosphorylated PGK1 were subjected to molecular dynamic simulation using the Amber 16 Molecular Dynamics package (http://ambermd.org/). We equilibrated the solvated complex by carrying out a short minimization, 50 ps of heating, and 50 ps of density equilibration with weak restraints on the complex, followed by 500 ps of constant pressure equilibration at 300 K. All simulations were run with shake on hydrogen atoms, a 2-fs time step and Langevin dynamics for temperature control. All trajectories were recorded every 5 ps for a total of 10 ns. The PTRAJ program in the Amber 16 package and VMD (Humphrey et al., 1996) were used to analyze the simulation results, including root-mean-square deviation, root-mean-square fluctuation, b-factor, and ΔG. The structural views of PGK1 were obtained using Discover Studio Visualizer and PyMOL (https://pymol.org/2/).

Docking of PTEN with PGK1 pY324 peptide

The docking between human PTEN (PDB: 1D5R) and Y324-phosphorylated PGK1 peptide (321-SKKpYAEA-327) was modeled using SeeSAR (https://www.biosolveit.de/SeeSAR/). The docking results were analyzed and adjusted with Discovery Studio Visualizer and SeeSAR and displayed with UCSF Chimera (http://www.cgl.ucsf.edu/chimera).

CRISPR/Cas9-mediated genomic editing

Genomic mutations were introduced into cells using a CRISPR/Cas9 system as described previously (Ran et al., 2013). Single guide RNAs (sgRNAs) were designed using the CRISPR Design tool (https://zlab.bio/guide-design-resources) and annealed by incubation at 95°C for 5 min and followed by cooling down to room temperature. The annealed sgRNA oligos were inserted into a PX458-Cas9-HF (high fidelity) vector digested by the *Bbs*I restriction enzyme (Kleinstiver et al., 2016). Cells (U87, U251, LN229, Pten$^{+/+}$, and Pten$^{-/-}$) were seeded at 60% confluence, followed by co-transfection of sgRNA (0.5 μg) with a single-stranded donor oligonucleotide (ssOND, 10 pmol) as a temple to introduce mutations, or without ssOND to introduce indel mutations. At 24 h after transfection, green fluorescent protein (GFP)-positive cells were sorted, and single cells were seeded into 96-well plates. Genomic DNA was extracted, followed by sequencing of the PCR products spanning the mutation sites. The ssOND and primers used for sgRNA cloning and genomic DNA sequencing were listed in Table S3.

Apoptosis analysis

Apoptotic cells were analyzed by using DAPI staining. Cells (1×10^5) were seeded in a 6-well plate overnight. Cells were then then fixed by direct addition of formaldehyde (final concentration 12%) to the culture medium. After fixation, the cells were stained with DAPI (1 μg/ml) for 5 min, followed by washing with PBS. Cells with condensed and/or fragmented chromatin were indicative of apoptosis and counted.

Terminal deoxynucleotidyl transferase dUTP nick end labeling (TUNEL) assay

Mouse tumor tissues were cut into 5-μm-thick sections. Apoptotic cells were counted using the DeadEnd Colorimetric TUNEL System (Promega) according to the manufacturer's instructions.

QUANTIFICATION AND STATISTICAL ANALYSIS

Statistical analyses were conducted with a two-tailed unpaired Student's t test unless specifically indicated. All data represent the mean ± standard deviation of three independent experiments/samples unless otherwise specified. Differences in means were considered statistically significant at $p < 0.05$. Significance levels are: * $p < 0.05$; ** $p < 0.001$; N.S., not significant. Analyses were performed using the Microsoft Excel.

DATA AND CODE AVAILABILITY

Raw data have been deposited to Mendeley Data and are available at https://doi.org/10.17632/3s8ny9vh85.1.

Molecular Cell, Volume *76*

Supplemental Information

PTEN Suppresses Glycolysis by Dephosphorylating and Inhibiting Autophosphorylated PGK1

Xu Qian, Xinjian Li, Zhumei Shi, Yan Xia, Qingsong Cai, Daqian Xu, Lin Tan, Linyong Du, Yanhua Zheng, Dan Zhao, Chuanbao Zhang, Philip L. Lorenzi, Yongping You, Bing-Hua Jiang, Tao Jiang, Haitao Li, and Zhimin Lu

SUPPLEMENTARY IMFORMATION

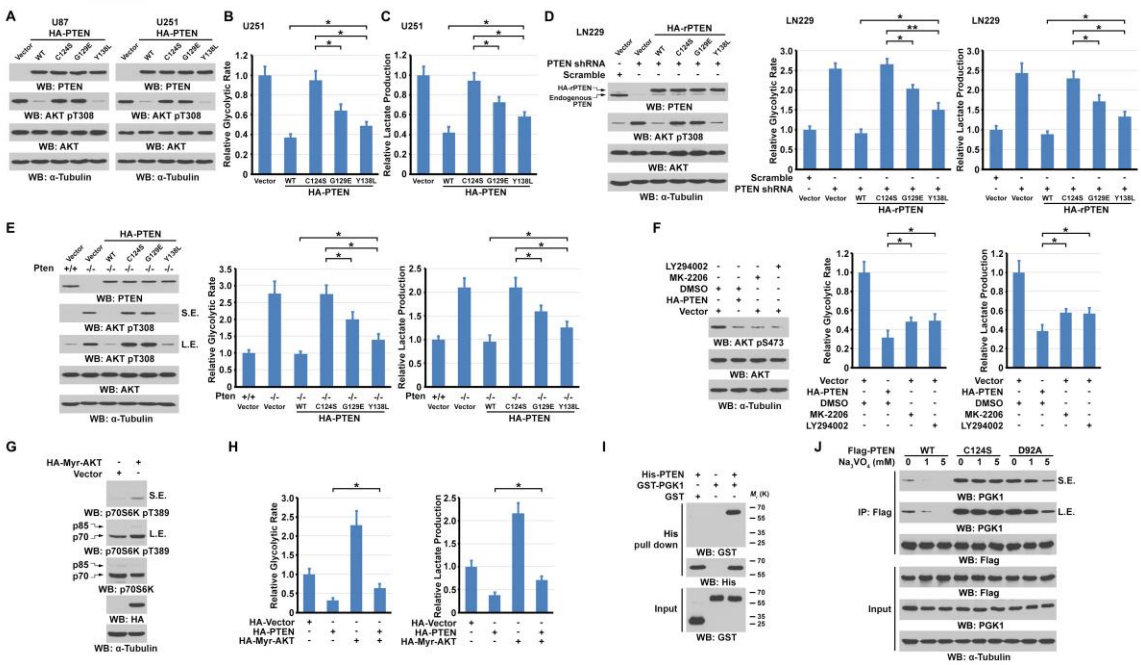

Figure S1. PTEN protein phosphatase activity regulates glycolysis, Related to Figure 1.

(A) HA-tagged WT PTEN, PTEN C124S, PTEN G129E, or PTEN Y138L mutant was expressed in U87 or U251 cells. Immunoblotting analyses were performed with the indicated antibodies.

(B, C) HA-tagged WT PTEN, PTEN C124S, PTEN G129E, or PTEN Y138L mutant was expressed in U251 cells. Glycolytic rate (B) and lactate production (C) were measured. Data represent the mean ± SD of triplicate experiments. * $P < 0.05$.

(D) LN229 cells, with or without PTEN depletion and reconstituted expression of HA-tagged WT shRNA-resistant (r) PTEN, rPTEN C124S, rPTEN G129E, or rPTEN Y138L, were cultured. Immunoblotting analyses were performed with the indicated antibodies (left panel). Glycolytic rate (middle panel) and lactate production (right panel) were measured

in the indicated cells. Data represent the mean ± SD of triplicate experiments. * $P < 0.05$; ** $P < 0.001$.

(E) HA-tagged WT PTEN, PTEN C124S, PTEN G129E, or PTEN Y138L mutant was expressed in $Pten^{-/-}$ MEFs. Immunoblotting analyses were performed with the indicated antibodies (left panel). Glycolytic rate (middle panel) and lactate production (right panel) were measured in the indicated cells. Data represent the mean ± SD of triplicate experiments. * $P < 0.05$. S.E., short exposure; L.E., long exposure.

(F) U87 cells transfected with or without HA-PTEN were treated with or without MK-2206 (5 μM) or LY294002 (20 μM) for 6 h. Immunoblotting analyses were performed with the indicated antibodies (left panel). Glycolytic rate (middle panel) and lactate production (right panel) were measured in the indicated cells. Data represent the mean ± SD of triplicate experiments. * $P < 0.05$.

(G) U87 cells were transfected with or without HA-Myr-AKT. Immunoblotting analyses were performed with the indicated antibodies.

(H) U87 cells were transfected with or without HA-PTEN or HA-Myr-AKT. Glycolytic rate (left panel) and lactate production (right panel) were measured in the indicated cells. Data represent the mean ± SD of triplicate experiments. * $P < 0.05$.

(I) A His pulldown assay with Ni-NTA agarose beads was performed by mixing bacterially purified His-PTEN with bacterially purified GST or GST-PGK1. No GST binding with His-PTEN was found.

(J) U87 cells transfected with WT Flag-PTEN, Flag-PTEN C124S, or Flag-PTEN D92A mutant were treated with or without the indicated concentration of sodium orthovanadate

(Na_3VO_4) for 6 h. Immunoprecipitation and immunoblotting analyses were performed with the indicated antibodies.

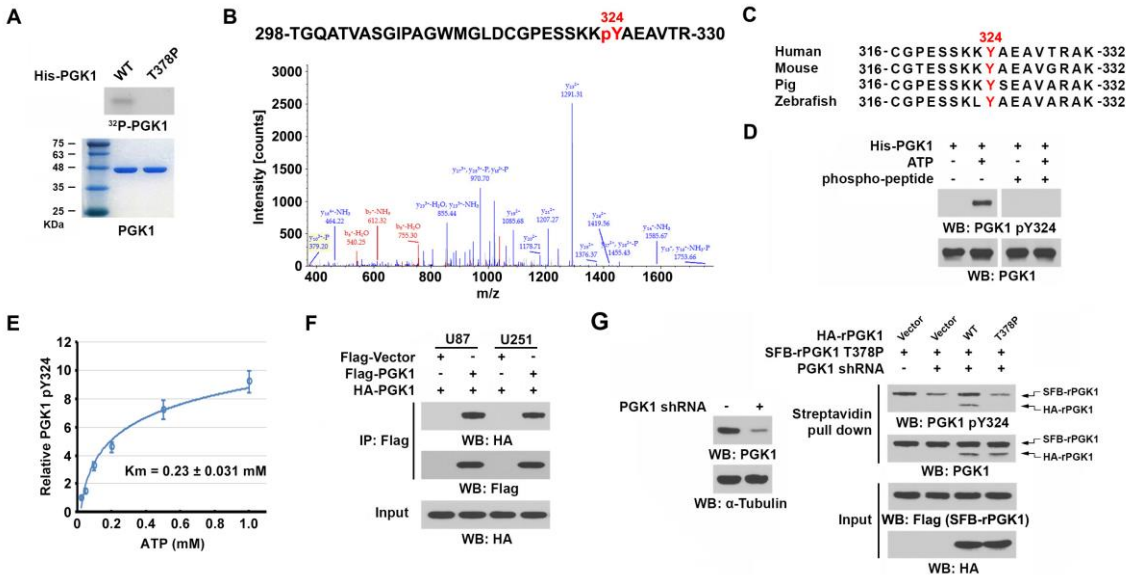

Figure S2. PGK1 is autophosphorylated at Y324, Related to Figure 2.

(D, F, and G) Immunoprecipitation or immunoblotting analyses were performed with the indicated antibodies.

(A) Purified WT His-PGK1 or a catalytically inactive His-PGK1 T378P mutant was incubated in the presence of [γ-^{32}P]-ATP. Autoradiography was performed (upper panel). Coomassie blue staining of proteins is shown (lower panel).

(B) Purified His-PGK1 was phosphorylated *in vitro* and analyzed by mass spectrometry. A mass spectrometric analysis was performed of a tryptic fragment at m/z 867.40167 Da (mass error was +5.55 ppm) matched to the +4 charged peptide 298-TGQATVASGIPAGWMGLDCGPESSKKYAEAVTR-330; the results suggested that Y324 was phosphorylated. The Mascot scores were 24, and the expectation value was 1.4e1.

(C) Alignment of PGK1 protein sequence spanning Y324 in different species.

(D) PGK1 Y324 phosphorylation-specific antibody was validated. Purified His-PGK1 was incubated in the presence or absence of ATP for autophosphorylation, which was followed by immunoblotting analyses with the indicated antibodies in the presence or absence of phospho-specific blocking peptide for the PGK1 pY324 antibody.

(E) Enzymatic kinetic plot of PGK1 Y324 autophosphorylation toward ATP is presented.

(F) HA-PGK1 with or without Flag-PGK1 were expressed in U87 or U251 cells.

(G) Endogenous PGK1-depleted U87 cells by PGK1 shRNA (left panel) were transfected with vectors expressing SFB-rPGK1 T378P with or without HA-tagged WT rPGK1 or rPGK1 T378P mutant. A streptavidin pulldown assay was performed.

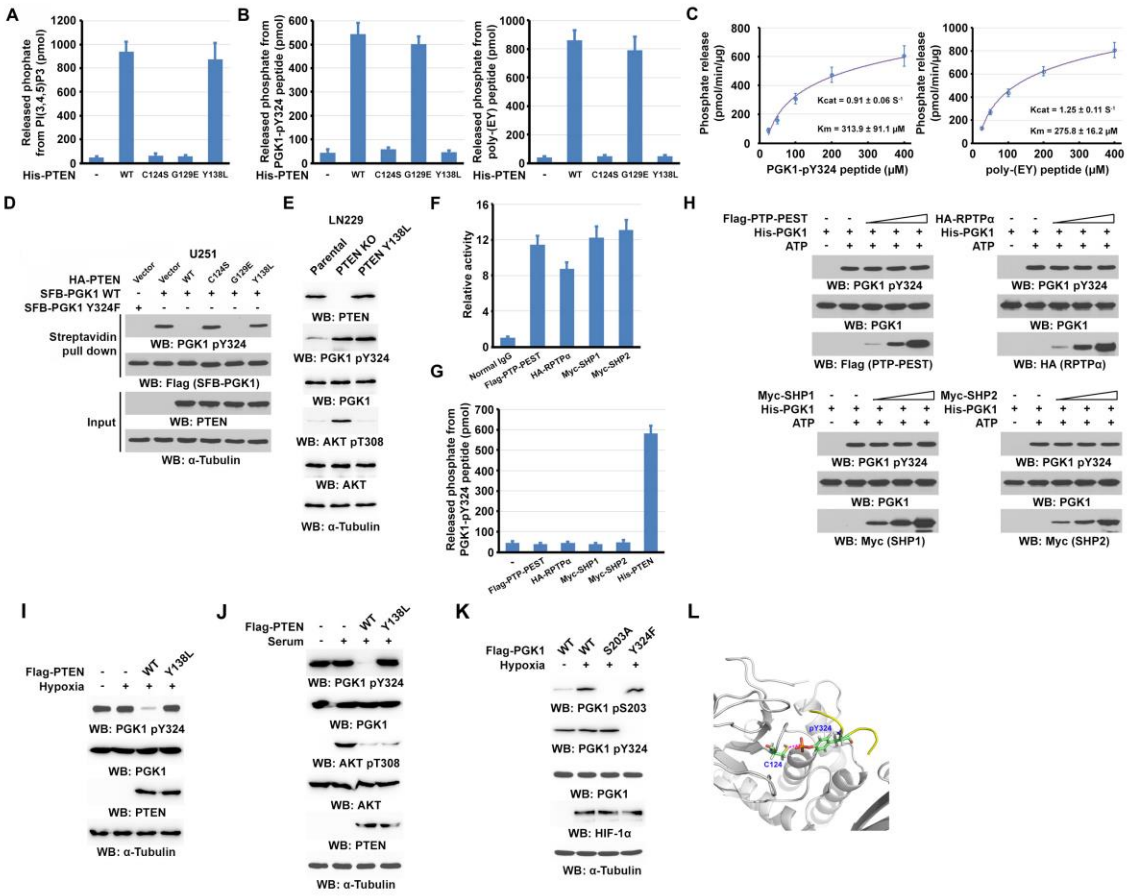

Figure S3. Autophosphorylated PGK1 is dephosphorylated by PTEN, Related to Figure 3.

(D, E, and H-K) Immunoblotting analyses were performed with the indicated antibodies.

(A, B) Purified WT His-PTEN, His-PTEN C124S, His-PTEN G129E, or His-PTEN Y138L mutant protein was incubated with PI(3,4,5)P3 (A), synthesized PGK1 peptide containing phospho-Y324 (B, left panel) or synthesized poly-(EY) peptide (B, right panel). The released phosphate was measured. Data represent the mean ± SD of triplicate samples.

(C) Enzymatic kinetic plot of purified His-PTEN toward synthesized PGK1 pY324 peptide (left panel) or synthesized poly-(EY) peptide (right panel).

(D) SFB-tagged WT PGK1 or PGK1 Y324F mutant with or without HA-tagged WT PTEN, PTEN C124S, PTEN G129E, or PTEN Y138L mutant were expressed in U251 cells. A streptavidin pulldown assay was performed.

(E) LN229 cells with or without PTEN knock-out (KO) or PTEN Y138L knock-in expression were lysed.

(F) Plasmids expressing the indicated phosphatases were transfected into 293T cells and immunoprecipitated with their corresponding tag antibodies. The phosphatase activities toward a common substrate, 3,6-fluorescein diphosphate (FDP), were measured. Data represent the mean ± SD of triplicate samples.

(G) The indicated phosphatases were transfected into 293T cells, immunoprecipitated with corresponding antibodies and competitively eluted and purified with their corresponding tag peptides. These phosphatases, along with bacterially purified His-PTEN, were incubated with the synthesized PGK1 peptide containing phospho-Y324. The released phosphate was measured. Data represent the mean ± SD of triplicate samples.

(H) Purified His-PGK1 immobilized on Ni-NTA agarose beads was incubated with or without ATP, followed by washing with PBS and incubation with or without the indicated purified phosphatases.

(I, J) U87 cells expressing with or without WT Flag-PTEN or Flag-PTEN Y138L were treated with or without hypoxia (1% O_2) for 24 h (I) or cultured with or without serum overnight (J).

(K) U87 cells expressing with or without WT Flag-PGK1, Flag-PGK1 S203A, or Flag-PGK1 Y324F were treated with or without hypoxia for 24 h.

(L) Detailed view showing a 3.5-Å distance between the $–PO_3$ group of phosphorylated PGK1 peptide and the –SH group of cysteine 124 of PTEN.

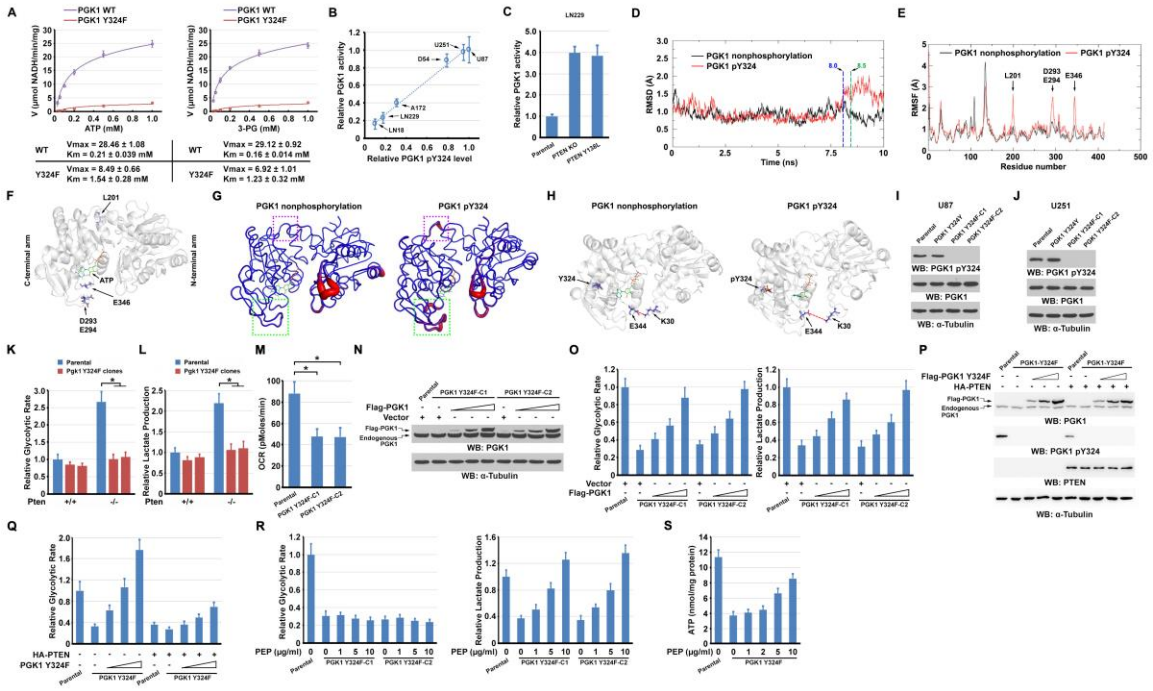

Figure S4. PTEN inhibits autophosphorylated PGK1, Related to Figure 4.

(A) Enzymatic kinetic plots of purified WT His-PGK1 and His-PGK1 Y324F mutant toward ATP (left panel) or 3-phosphoglycerate (3-PG, right panel) are presented.

(B) The activities of PGK1 purified from the indicated GBM cells were measured, and were normalized to that in U87 cells. The correlation between relative PGK1 activities and relative PGK1 pY324 levels (obtained from Figure 1F) in GBM cells were plotted.

(C) The activities of PGK1 purified from LN229 cells with or without PTEN knock-out (KO) or PTEN Y138L knock-in expression were measured using ADP as substrates. Data represent the mean ± SD of triplicate experiments.

(D) Backbone root-mean-square deviation (RMSD) of nonphosphorylated and Y324-phosphorylated PGK1 as a function of time. ns, nanosecond.

(E) Root-mean-square fluctuation (RMSF) of nonphosphorylated and Y324-phosphorylated PGK1 (PDB: 2Y3I). Highly different fluctuated amino acid residues are indicated.

(F) Labeling of highly different fluctuated amino acid residues in PGK1 (PDB: 2Y3I). These residues are shown as sticks.

(G) B-factor structures of nonphosphorylated and Y324-phosphorylated PGK1 based on molecular dynamic simulation. Highly fluctuated regions are highlighted in red. The purple dashed box (indicating the hinge-bending area) and the green dashed box (indicating the ATP binding area) denote the most different fluctuated areas in nonphosphorylated and Y324-phosphorylated PGK1.

(H) Distance measurement of the N-terminal and C-terminal arms in nonphosphorylated and Y324-phosphorylated PGK1. Residues including K30 in the N-terminal arm and Y324, pY324 and E344 in the C-terminal arm are shown as sticks.

(I, J) Immunoblotting analyses were performed with the indicated antibodies.

(K) $Pten^{+/+}$ or $Pten^{-/-}$ MEFs and the indicated clones with knock-in of PGK1 Y324F were incubated with D-[5-^{3}H]-glucose (10 μCi) for 1 h. The amount of diffused ^3H_2O converted from D-[5-^{3}H]-glucose was determined via scintillation counting. Data represent the mean ± SD of triplicate experiments. * $P < 0.05$.

(L) Lactate production was determined. Data represent the mean ± SD of triplicate experiments. * $P < 0.05$.

(M) The oxygen consumption rate (OCR) of U87 cells with or without PGK1 Y324F knock-in expression was measured. Data represent the mean ± SD of triplicate experiments. * $P < 0.05$. C1, clone 1; C2, clone 2.

(N, O) U87 cells with or without PGK1 Y324F knock-in were transfected with or without different amounts of Flag-PGK1. Immunoblotting analyses were performed with the indicated antibodies (N). Glycolytic rate (left panel) and lactate production (right panel) were measured (O). Data represent the mean ± SD of triplicate experiments.

(P, Q) U87 cells with or without PGK1 Y324F knock-in expression were transfected with or without HA-PTEN and different amounts of Flag-PGK1 Y324F mutant. Immunoblotting analyses were performed with the indicated antibodies (P). Cells were incubated with D-[5-^{3}H]-glucose (10 μCi) for 1 h. Glycolytic rates were determined (Q). Data represent the mean ± SD of triplicate experiments.

(R) U87 cells with or without PGK1 Y324F knock-in were treated with the indicated amounts of phosphoenolpyruvate (PEP) for 6 h. Glycolytic rate (left panel) and lactate production (right panel) were measured. Data represent the mean ± SD of triplicate experiments.

(S) U87 cells with or without PGK1 Y324F knock-in expression were treated with the indicated amounts of phosphoenolpyruvate (PEP) for 6 h. ATP levels were measured. Data represent the mean ± SD of triplicate experiments.

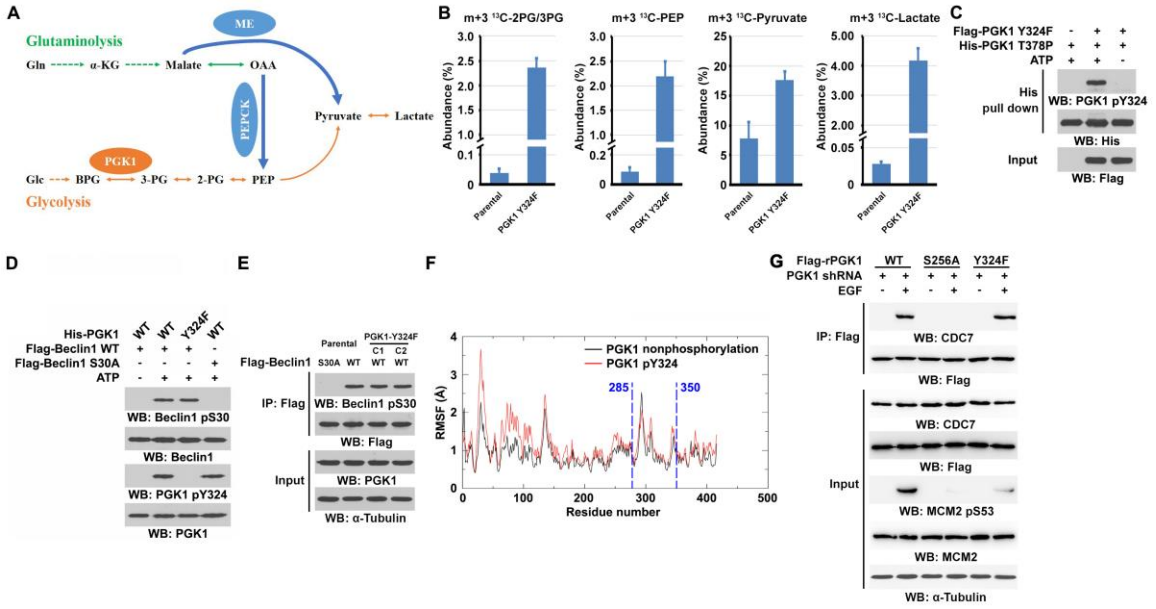

Figure S5. Y324 phosphorylation of PGK1 alters incorporation of glutamine to glycolysis and does not affect its protein kinase activity, Related to Figure 4.

(A) Diagram of glutamine metabolism into glycolysis. Gln, glutamine; α-KG, α-ketoglutarate; OAA, oxaloacetate; Glc, glucose; BPG, 1,3-biphosphoglycerate; 3-PG, 3-phosphoglycerate; 2-PG, 2-phosphoglycerate; PEP, phosphoenolpyruvate; ME, malate enzyme; PEPCK, phosphoenolpyruvate carboxykinase. Dashed arrows indicate multiple reaction steps; solid arrows indicate one reaction step; double-head arrows indicate reversible reactions.

(B) U87 cells with or without PGK1 Y324F knock-in were cultured in the presence of 5 mM glucose and labeled with 4 mM $^{13}C_5$-glutamine for 6 h. m+3 ^{13}C-labeled glycolytic

metabolites were measured by LC/MS-MS. Data represent the mean ± SD of triplicate experiments.

(C) An *in vitro* kinase assay was performed by mixing purified Flag-PGK1 Y324F and purified His-PGK1 T378P mutant. A His pulldown assay with Ni-NTA agarose beads was performed and followed by immunoblotting analyses with the indicated antibodies.

(D) An *in vitro* kinase assay was performed by mixing purified WT His-PGK1 or His-PGK1 Y324F mutant with purified WT Flag-Beclin1 or Flag-Beclin1 S30A. Immunoblotting analyses were performed with the indicated antibodies.

(E) U87 cells with or without PGK1 Y324F knock-in were transfected with or without WT Flag-Beclin1 or Flag-Beclin1 S30A and cultured in the absence of glucose for 12 h. Immunoprecipitation and immunoblotting analyses were performed with the indicated antibodies.

(F) Root-mean-square fluctuation (RMSF) of nonphosphorylated and Y324-phosphorylated PGK1 (PDB: 1VJD). aa285-350 indicates the ATP binding area.

(G) U251 cells with PGK1 depletion and reconstituted expression of WT Flag-rPGK1, Flag-rPGK1 S256A, or Flag-rPGK1 Y324F were serum starved overnight, followed by treatment with or without 100 ng/ml of EGF for 30 min. Immunoprecipitation and immunoblotting analyses were performed with the indicated antibodies.

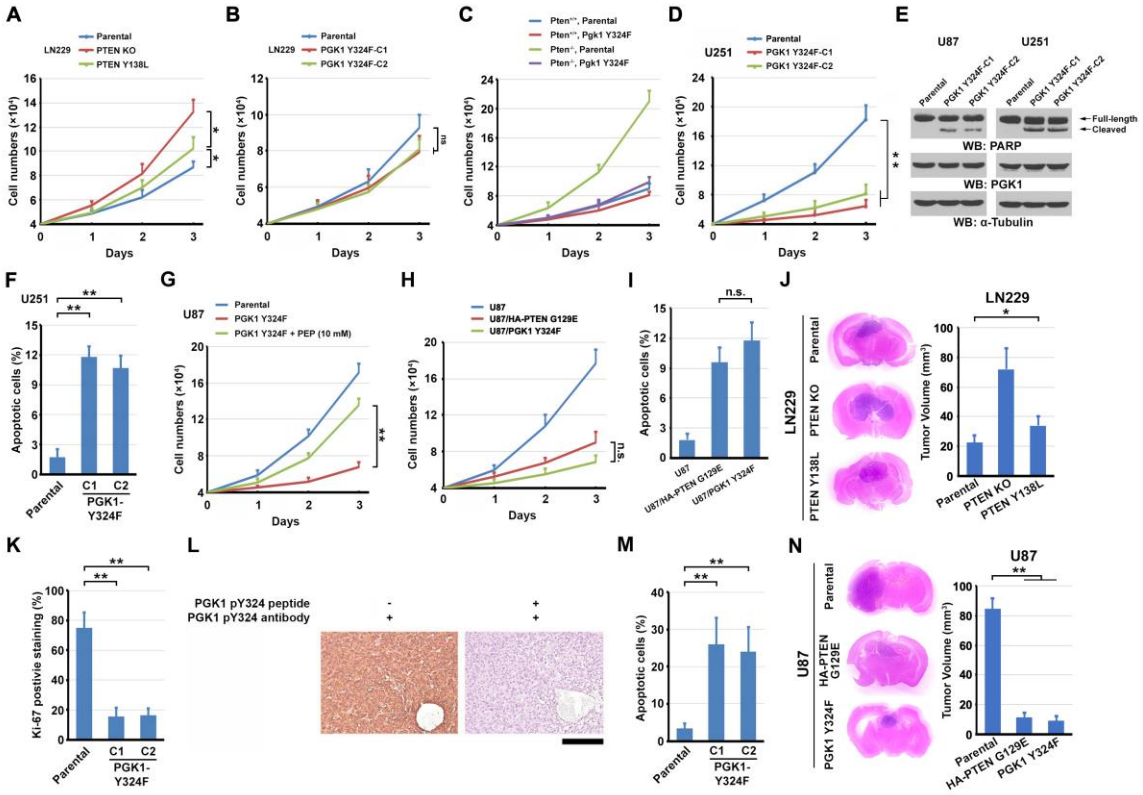

Figure S6. PGK1 autophosphorylation is instrumental for brain tumor growth, Related to Figure 5.

(A) LN229 cells with or without PTEN knock-out (KO) or PTEN Y138L knock-in were incubated for the indicated period of time. Cell numbers were counted. Data represent the mean ± SD of triplicate samples. * $P < 0.05$.

(B) LN229 cells with or without knock-in of PGK1 Y324F were cultured for the indicated periods of time. Cell numbers were counted. Data represent the mean ± SD of triplicate samples. ns, no significance. C1, clone 1; C2, clone 2.

(C) $Pten^{+/+}$ or $Pten^{-/-}$ MEFs with or without knock-in expression of Pgk1 Y324F were cultured for the indicated periods of time. Cell numbers were counted. Data represent the mean ± SD of triplicate samples.

(D) U251 cells (4×10^4) with or without knock-in of PGK1 Y324F were cultured for the indicated periods of time. Cell numbers were counted. Data represent the mean ± SD of triplicate samples. ** $P < 0.001$.

(E) Immunoblotting analyses were performed with the indicated antibodies.

(F) Apoptosis analyses were performed using U251 cells with or without PGK1 Y324F knock-in expression. Data represent the mean ± SD of triplicate experiments. ** $P < 0.001$.

(G) U87 cells with or without knock-in of PGK1 Y324F were cultured in the presence or absence of PEP for the indicated periods of time. Cell numbers were counted. Data represent the mean ± SD of triplicate samples. ** $P < 0.001$.

(H, I) U87 cells with or without HA-PTEN G129E or PGK1 Y324F knock-in expression were cultured for the indicated periods of time. Cell numbers were counted (H). Apoptosis analyses were performed (I). Data represent the mean ± SD of triplicate samples. n.s., no significance.

(J) LN229 cells with or without PTEN knock-out (KO) or PTEN Y138L knock-in were intracranially injected into athymic nude mice (n =5 per group). Mice were sacrificed and examined for tumor growth 28 days after injection. Representative H&E-stained brain sections are shown (left panel). Tumor volumes were calculated (right panel). Data represent the mean ± SD of 5 mice in each group. * $P < 0.05$.

(K) Ki-67 positvie cells were quantified, and the data represent the mean ± SD from 10 randomly selectived microscope fields (right panel). ** $P < 0.001$.

(L) The antibody specificity was validated. IHC staining of mouse tumor tissues were performed with a specific antibody against PGK1 pY324 with or without mixing with its specific phospho-blocking peptide. Scale bar, 100 μm.

(M) Apoptotic cells were quantified, and the data represent the mean ± SD from 10 randomly selectived microscope fields. ** $P < 0.001$.

(N) U87 cells with or without HA-PTEN G129E or PGK1 Y324F knock-in expression were intracranially injected into athymic nude mice (n =5 per group). Mice were sacrificed and examined for tumor growth 28 days after injection. Representative H&E-stained brain sections are shown (left panel). Tumor volumes were calculated (right panel). Data represent the mean ± SD of 5 mice in each group. ** $P < 0.001$.